Macrophage-derived IL-6 trans-signalling as a novel target in the pathogenesis of bronchopulmonary dysplasia

Dharmesh Hirani[1,2], Cristina M. Alvira[3], Soula Danopoulos[4], Carlos Milla[3], Michele Donato[5], Lu Tian[6], Jasmine Mohr[1,2], Katharina Dinger[1,2], Christina Vohlen[1,7], Jaco Selle[1], Silke v. Koningsbruggen-Rietschel[7], Verena Barbarino[8], Christian Pallasch[8], Stefan Rose-John[9], Margarete Odenthal[10], Gloria S. Pryhuber[11], Siavash Mansouri[12], Rajkumar Savai[12,13], Werner Seeger[12,13], Purvesh Khatri[5], Denise Al Alam[4], Jörg Dötsch[7] and Miguel A. Alejandre Alcazar[1,2,13,14]

[1]University of Cologne, Faculty of Medicine and University Hospital Cologne, Translational Experimental Pediatrics - Experimental Pulmonology, Dept of Pediatric and Adolescent Medicine, Cologne, Germany. [2]University of Cologne, Faculty of Medicine and University Hospital Cologne, Center for Molecular Medicine Cologne (CMMC), Cologne, Germany. [3]Dept of Pediatrics, Stanford University School of Medicine, Stanford, CA, USA. [4]Lundquist Institute for Biomedical Innovation at Harbor-UCLA Medical Center, Torrance, CA, USA. [5]Biomedical Informatics Research-Institute for Immunity, Transplantation, and Infection, Stanford University, Stanford, CA, USA. [6]Dept of Biomedical Data Science, Stanford University, Stanford, CA, USA. [7]University of Cologne, Faculty of Medicine and University Hospital Cologne, Dept of Pediatric and Adolescent Medicine, Cologne, Germany. [8]Dept I of Internal Medicine, Center for Integrated Oncology (CIO) Köln-Bonn, University of Cologne, Cologne, Germany. [9]Institute of Biochemistry, Christian-Albrechts-University Kiel, Kiel, Germany. [10]University of Cologne, Faculty of Medicine and University Hospital Cologne, Institute for Pathology, Cologne, Germany. [11]Division of Neonatology, Dep of Pediatrics, University of Rochester Medical Center, Rochester, NY, USA. [12]Dept of Lung Development and Remodeling, Max-Planck-Institute for Heart and Lung Research, Member of the German Center for Lung Research (DZL), Bad Nauheim, Germany. [13]Institute for Lung Health (ILH), University of Giessen and Marburg Lung Center (UGMLC), Member of the German Center for Lung Research (DZL), Giessen, Germany. [14]University of Cologne, Faculty of Medicine and University Hospital Cologne, Cologne Excellence Cluster on Stress Responses in Aging-associated Diseases (CECAD), Cologne, Germany.

Corresponding author: Miguel Alejandre Alcázar (miguel.alejandre-alcazar@uk-koeln.de)

Shareable abstract (@ERSpublications)
M1-like macrophage activation is linked to IL-6/STAT3 axis in clinical and experimental BPD. Inhibition of macrophage-related IL-6 trans-signalling promotes ATII survival and lung growth in experimental BPD as a new therapy for preterm infants. https://bit.ly/3AhF7GP

Cite this article as: Hirani D, Alvira CM, Danopoulos S, *et al*. Macrophage-derived IL-6 trans-signalling as a novel target in the pathogenesis of bronchopulmonary dysplasia. *Eur Respir J* 2022; 59: 2002248 [DOI: 10.1183/13993003.02248-2020].

Received: 12 June 2020
Accepted: 24 June 2021

Abstract

Rationale Premature infants exposed to oxygen are at risk for bronchopulmonary dysplasia (BPD), which is characterised by lung growth arrest. Inflammation is important, but the mechanisms remain elusive. Here, we investigated inflammatory pathways and therapeutic targets in severe clinical and experimental BPD.

Methods and results First, transcriptomic analysis with *in silico* cellular deconvolution identified a lung-intrinsic M1-like-driven cytokine pattern in newborn mice after hyperoxia. These findings were confirmed by gene expression of macrophage-regulating chemokines (*Ccl2*, *Ccl7*, *Cxcl5*) and markers (*Il6*, *Il17A*, *Mmp12*). Secondly, hyperoxia-activated interleukin 6 (IL-6)/signal transducer and activator of transcription 3 (STAT3) signalling was measured *in vivo* and related to loss of alveolar epithelial type II cells (ATII) as well as increased mesenchymal marker. *Il6* null mice exhibited preserved ATII survival, reduced myofibroblasts and improved elastic fibre assembly, thus enabling lung growth and protecting lung function. Pharmacological inhibition of global IL-6 signalling and IL-6 trans-signalling promoted alveolarisation and ATII survival after hyperoxia. Third, hyperoxia triggered M1-like polarisation, possibly *via* Krüppel-like factor 4; hyperoxia-conditioned medium of macrophages and IL-6-impaired ATII proliferation. Finally, clinical data demonstrated elevated macrophage-related plasma cytokines as potential biomarkers that identify infants receiving oxygen at increased risk of developing BPD. Moreover, macrophage-derived *IL6* and active STAT3 were related to loss of epithelial cells in BPD lungs.

Conclusion We present a novel IL-6-mediated mechanism by which hyperoxia activates macrophages in immature lungs, impairs ATII homeostasis and disrupts elastic fibre formation, thereby inhibiting lung growth. The data provide evidence that IL-6 trans-signalling could offer an innovative pharmacological target to enable lung growth in severe neonatal chronic lung disease.

Introduction

Premature infants often require respiratory support, including mechanical ventilation and/or supplemental oxygen. However, these life-saving treatments when applied to the immature lung can impair lung growth, leading to neonatal chronic lung disease, initially described as bronchopulmonary dysplasia (BPD) [1]. Lungs of infants afflicted with BPD are typically characterised by reduced formation of alveoli and perturbed matrix remodelling, yielding structural changes that may persist beyond adolescence [2, 3]. Despite significant advances in neonatal management over the past decades, the incidence of BPD remains high, with a lack of effective preventive or therapeutic strategies. Thus, identifying new molecular pathways that impair alveolar growth and regeneration after injury of the immature lung may lead to potential novel therapeutics.

Alveolar epithelial type I (ATI) and type II (ATII) cells lining the alveoli are injured when exposed to hyperoxia and this likely contributes to the pathogenesis of BPD [4, 5]. Alveolar regeneration is primarily directed by ATII, which have the capacity for self-renewal and give rise to ATI after lung injury [6]. Disruption of ATII homeostasis is involved in the pathogenesis of various chronic lung diseases, including BPD [7, 8]. Hyperoxia reduces survival and induces epithelial mesenchymal transition in ATII [9, 10]. Growth factors and cytokines can modulate ATII homeostasis, reducing alveolar formation and regeneration [10, 11]. Thus, changes in the pulmonary microenvironment after hyperoxia may complicate the course of BPD by decreasing ATII survival and alveolar growth.

The pathogenesis of BPD also includes changes in immune cell proportions, but the mechanisms and the role of distinct immune cells in BPD pathogenesis are not yet known [12, 13]. Recent studies demonstrated that resident and non-resident macrophages are key constituents of the inflammatory lung environment in response to injury, orchestrating it through secretion of various cytokines, including interleukin 6 (IL-6), a regulator of cell homeostasis, matrix remodelling, immune response and tissue regeneration [14]. On the other hand, macrophages also contribute to a regenerative niche, essential for repair after lung injury [15]. Anti-inflammatory approaches attenuate impaired alveolarisation induced by hyperoxia [16, 17]. However, the impact of oxygen on the regulation of the inflammatory lung microenvironment as well as its impact on ATII homeostasis and alveolar formation remain elusive.

In this study, we present evidence that prolonged oxygen exposure recapitulates severe neonatal chronic lung disease, activates macrophages, favouring M1-like polarisation, and increases IL-6 activity in newborn lungs. Of note, we demonstrate that specific blockade of IL-6 trans-signalling preserves ATII survival and enables lung growth after hyperoxia. Mechanistically, we show that the secretome of hyperoxia-exposed macrophages inhibits ATII survival, and we identify a possible novel role for the transcription factor Krüppel-like factor 4 (Klf4) in accentuating the macrophage response after hyperoxia. In human cell culture studies, we demonstrate that hyperoxia-activated pro-inflammatory M1-like macrophages have an additive effect on hyperoxia-reduced survival of human alveolar epithelial cells (hAECs). Finally, we confirm that the macrophage-driven inflammatory IL-6/ signal transducer and activator of transcription 3 (STAT3) response is present in lungs or in the serum of infants with BPD.

Material and methods

Extended descriptions of the materials and methods are provided in the supplementary material.

Animal experiments

Animals studies were divided into four groups: 1) exposure of male and female newborn mice on a C57Bl6 background to hyperoxia (80% O_2) for 14 days for transcriptomic analysis of whole lungs, and to 40% or 85% O_2 for 3, 7 or 28 days for subsequent assessment of IL-6 signalling; 2) exposure of newborn C57BL6 mice as well as 3) newborn B6.129S2-*Il6*$^{tm1Kopf/J}$ (*Il6*$^{-/-}$) and their respective wildtype (WT) control to hyperoxia (85% O_2) for 28 days to determine long-term effects of hyperoxia. Finally, 4) newborn mice were treated intraperitoneally with soluble gp130Fc or IL-6 mAb at postnatal days (P) 2, P7, P14, and 21. See details and descriptions of pulmonary function tests in the supplementary material.

Tissue assays

RNA extraction, mRNA measurement

RNA extraction and quantitative real-time PCR were performed as previously described [18].

Transcriptomic analysis using RNA sequencing, bioinformatics analyses and in silico cellular deconvolution

All statistical analyses were obtained with the R statistical framework. Pathway analysis was performed on *Mus musculus* pathways from the Kyoto Encyclopedia of Genes and Genomes (KEGG) and StringDB databases [19]. *In silico* cellular deconvolution was performed using the immunoStates method [20].

Protein extraction and immunoblots

Protein extraction, protein measurements and immunoblots were performed as described previously [18]. Antibodies are listed in the supplementary material.

Postmortem processing of lungs for quantitative histology immunostaining

Septal thickness, mean linear intercept, radial alveolar count, surface of a single alveolus, insoluble lung elastin and microvessels were assessed as described previously [21] and in detail in the supplementary material. Lungs were stained for CD68 (macrophages), α-smooth muscle actin (αSMA^{+}) (myofibroblasts), pro-surfactant protein C (SFTPC) (ATII) and cell death (terminal deoxynucleotidyl transferase dUTP nick end labelling (TUNEL)). Positive stained cells were counted as detailed in the supplementary material.

Cell culture studies

Cell lines, reagents and assays

Murine lung epithelial cells (MLE12; American Type Culture Collection), macrophages (J774A.1; American Type Culture Collection), primary murine macrophages (peritoneal) from WT mice, human monocyte-derived macrophages from donors and hAECs (CellBiologics; PELOBiotech, Germany) were studied. For ethical consent and detailed information, please see the supplementary material. MLE12 and hAECs were exposed to mouse or human IL-6 (Sigma-Aldrich, Germany)+mouse or human IL-6Ra (IL-6Ra protein, R&D Systems, USA) (IL-6/soluble IL-6 receptor (sIL-6R)). Proliferation was assessed using MTT assay (ATCC; No. 30-1010K). IL-6 was measured using ELISA (IL-6 ELISA, Invitrogen, USA). Klf4 was silenced in macrophages (J774.A1) with small interfering klf4 (Dharmacon, Cat. No. SO-2589106G, USA) using Endo-Porter (GeneTools LLC, Philomath, USA).

Precision-cut lung slices (PCLS)

Murine lungs were isolated from the 14-day-old mice after intratracheal instillation of agarose. PCLS were treated with IL-6 (Sigma-Aldrich, Germany)+20 ng IL-6Ra (IL-6Ra Protein, R&D Systems, USA) (IL-6/sIL-6R) under normoxia (21% O_2) or hyperoxia (85% O_2) for 48 h. Subsequently, PCLS were fixed with 4% paraformaldehyde and paraffin-embedded for immunofluorescence staining for SFTPC and TUNEL detection (*in situ* Cell Death Detection Kit, Roche, Germany).

Human lung tissue

BPD and control (non-diseased) lung tissues were obtained through the National Heart, Lung, and Blood Institute LungMAP Consortium Human Tissue Core Biorepository. The biorepository is approved by the University of Rochester Research Subjects Review Board (RSRB00056775). Consent for research use has been provided for each sample. Clinical metadata and histopathology are listed in table 1.

Immunostaining of human lungs

BPD and control lungs were stained for pSTAT3 (1:200; Cell Signaling, no. 9145), CD45 (1:200; Invitrogen, 14-9457-82), cadherin 1 (1:200, BD Biosciences, 610181), CD68 (1:200, eBioscience, 14-0688-82) and SFTPC (1:100, LSBio, LS-B10952).

In situ hybridisation of human lungs

Fluorescent *in situ* hybridisation for *Il6* was conducted using the Advanced Cell Diagnostics RNAscope Fluorescent Multiplex Assay.

Clinical studies

55 infants born at <32 weeks gestation were enrolled into a longitudinal cohort of patients at Lucile Packard Children's Hospital. Stanford University's Institutional Review Board approved the study. Informed parental consent was granted for each infant enrolled in the study. Infants were followed up to 36 weeks post-menstrual age. Plasma samples were assayed for cytokine profiling by 63-plex bead assay. Clinical data are summarised in supplementary table S2.

Statistical analysis

All continuous measurements are expressed as mean±standard error of the mean and $p<0.05$ denoted significant differences. For *in vivo* murine studies, Two-way ANOVA or one-way ANOVA followed by a

TABLE 1 Clinical data of lungs of infants with and without bronchopulmonary dysplasia (BPD)

Healthy human sample				
Donor ID	**Calculated age (months)**	**Sex**	**Race**	**ClinPathDx: control**
D075	4.00	Male	White	Normal growth and development
D031	7.64	Male	White	Normal growth and structure
D090	14.70	Female	NR	Normal growth and structure
D046	36.5	Male	White	Normal growth and development
D139	47.67	Female	One race	Normal lung growth and structure
D056	68.21	Male	White	Normal growth and development
BPD human sample				
Donor ID	**Calculated age (months)**	**Sex**	**Race**	**ClinPathDx: BPD/CLD**
D029	3.55	Male	White	23 weeks at birth, histology: CLD/BPD with lobular remodelling; mild medial hypertrophy of small arteries
D086	8.94	Male	White	25 weeks at birth, probable BPD with respiratory failure
D141	13.40	Male	White	25 weeks at birth, BPD; moderate deficient alveolarisation, chronic inflammation, airway muscle hyperplasia, medial hypertrophy of small arteries
D039	39.13	Female	NR	23 weeks at birth, "new" BPD
D053	37.87	Male	White	24 weeks at birth, BPD, mild-moderate bronchiolitis
D055	59.96	Male	White	32 weeks at birth, possible mild BPD, asthma, moderate bronchopneumonia

NR: not reported; CLD: chronic lung disease; ClinPathDx: clinical pathology diagnostic.

Dunn's or Bonferroni's post-test, respectively, Mann–Whitney test and t-test were used to test for statistical significance. For cell culture studies, we applied (repeated measures) one-way ANOVA followed by a Bonferroni's post-test or paired t-test. For human studies, we used Mann–Whitney test, t-test, a non-parametric fitted curve and a mixed linear model.

Results

Transcriptomic analysis identifies chemokine signalling as the most regulated pathway in murine lungs after hyperoxia

RNA sequencing transcriptomic profiling was performed as depicted in figure 1a. Genes with average log-fold change greater than two and a false discovery rate-corrected p-value <0.01 were considered as differentially expressed genes (DEGs) (figure 1b, c). Pathway analysis on the KEGG pathway database identified a number of relevant pathways. Of these, the most notable were the cytokine-cytokine receptor interaction and chemokine-mediated signalling pathway (figure 1d). To identify putative functional networks, we used DEGs in the ten most up- and down-regulated KEGG pathways as input for StringDB (figure 1e–h). First, we identified the ten most significant biological processes (figure 1e) and molecular functions (figure 1f) using gene ontology analysis. Secondly, based on DEGs in the ten most regulated KEGG pathways, we generated a functional network (figure 1h), which highlighted the centrality of DEGs. Each DEG in the functional network has a colour-code, which allows the individual assignment to the biological processes shown in figure 1e. We next defined a ranking for the centrality of each DEG and identified the top ten hubs. Of these hubs, nine are chemokines related to macrophage function (figure 1g).

In silico *cellular deconvolution identifies inflammatory immune cell dysregulation in neonatal lungs after hyperoxia*

We next applied the immunoStates method to the gene expression data to assess if any immune cell type showed different proportions in hyperoxia compared to normoxia. Myeloid dendritic cells, naïve B cells, and plasma cells were increased; whereas $CD4^+$, $CD56^+$ and mast cells were significantly reduced. Consistent with our hypothesis, pro-inflammatory M1-like macrophages proportions were higher in the hyperoxia group. In contrast, activated, anti-inflammatory M2-like macrophages proportions were lower (figure 2a, b). We confirmed these findings using quantitative real-time PCR to determine the expression of key macrophage-regulating markers (*Ccl7*, *Cxcl5* and *Ccl2*) (figure 2c). Furthermore, hyperoxia

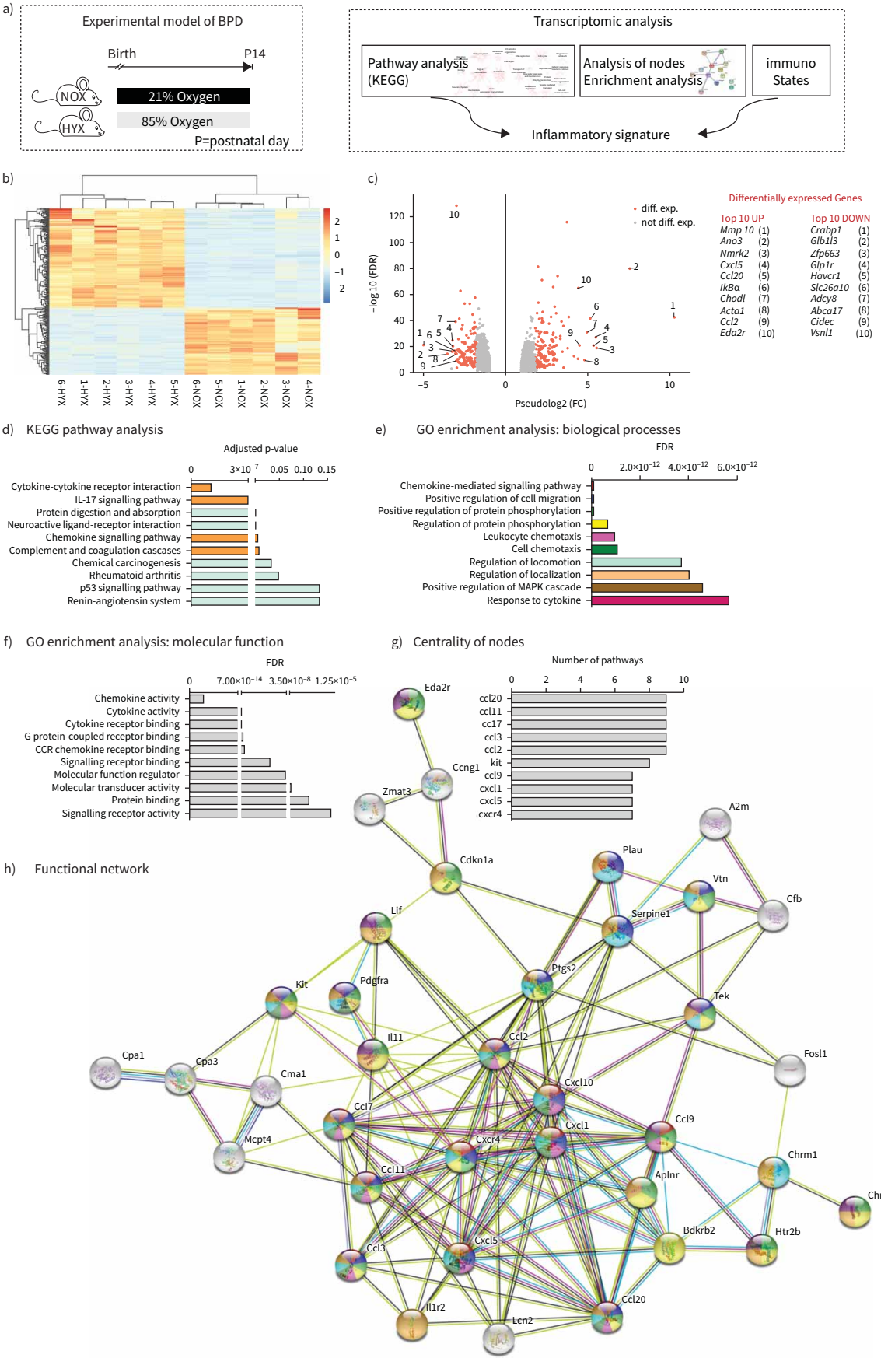
a)
Experimental model of BPD
Birth
P14
NOX
HYX
21% Oxygen
85% Oxygen
P=postnatal day
Transcriptomic analysis
Pathway analysis (KEGG)
Analysis of nodes Enrichment analysis
immuno States
Inflammatory signature
b)
6-HYX
1-HYX
2-HYX
3-HYX
4-HYX
5-HYX
6-NOX
5-NOX
1-NOX
2-NOX
3-NOX
4-NOX
c)
diff. exp.
not diff. exp.
−log 10 (FDR)
Pseudolog2 (FC)
Differentially expressed Genes
Top 10 UP
Mmp 10 (1)
Ano3 (2)
Nmrk2 (3)
Cxcl5 (4)
Ccl20 (5)
IkBα (6)
Chodl (7)
Acta1 (8)
Ccl2 (9)
Eda2r (10)
Top 10 DOWN
Crabp1 (1)
Glb1l3 (2)
Zfp663 (3)
Glp1r (4)
Havcr1 (5)
Slc26a10 (6)
Adcy8 (7)
Abca17 (8)
Cidec (9)
Vsnl1 (10)
d) KEGG pathway analysis
Adjusted p-value
Cytokine-cytokine receptor interaction
IL-17 signalling pathway
Protein digestion and absorption
Neuroactive ligand-receptor interaction
Chemokine signalling pathway
Complement and coagulation cascades
Chemical carcinogenesis
Rheumatoid arthritis
p53 signalling pathway
Renin-angiotensin system
e) GO enrichment analysis: biological processes
FDR
Chemokine-mediated signalling pathway
Positive regulation of cell migration
Positive regulation of protein phosphorylation
Regulation of protein phosphorylation
Leukocyte chemotaxis
Cell chemotaxis
Regulation of locomotion
Regulation of localization
Positive regulation of MAPK cascade
Response to cytokine
f) GO enrichment analysis: molecular function
FDR
Chemokine activity
Cytokine activity
Cytokine receptor binding
G protein-coupled receptor binding
CCR chemokine receptor binding
Signalling receptor binding
Molecular function regulator
Molecular transducer activity
Protein binding
Signalling receptor activity
g) Centrality of nodes
Number of pathways
ccl20
ccl11
cc17
ccl3
ccl2
kit
ccl9
cxcl1
cxcl5
cxcr4
h) Functional network
Eda2r
Ccng1
Zmat3
A2m
Plau
Cdkn1a
Vtn
Cfb
Lif
Serpine1
Ptgs2
Kit
Pdgfra
Tek
Il11
Ccl2
Fosl1
Cpa1
Cpa3
Cma1
Cxcl10
Ccl7
Ccl9
Mcpt4
Cxcr4
Cxcl1
Chrm1
Ccl11
Aplnr
Chrna7
Bdkrb2
Htr2b
Ccl3
Cxcl5
Ccl20
Il1r2
Lcn2

FIGURE 1 Transcriptomic analyses of lungs of newborn mice exposed to normoxia (21% O_2, NOX) or hyperoxia (80% O_2, HYX) for 14 days (a), heatmap (b) and volcano plot (c). The heatmap contains only genes with an average log-fold change (FC) greater than 2 and false discovery rate (FDR)-corrected p-value <0.01. Genes with average log-FC greater than 2 and FDR-corrected p-value <0.01 were considered as differentially expressed (diff. exp.) genes and they are colored red. Labels in the volcano plot indicate top 10 up- and down-regulated genes based on FC; n=6 per group; NOX, normoxia (21% O_2); HYX, hyperoxia (80% O_2). d) Kyoto Encyclopedia of Genes and Genomes (KEGG) pathway analysis showing the top ten pathways dysregulated in lungs of newborn mice exposed to NOX or HYX for 14 days. e–h) Functional enrichment analysis to identify functional gene sets, including biological processes (e) and molecular functions (f) using differentially expressed genes identified in the top 10 pathways of the KEGG pathway analysis. Ranking of the DEGs (g) identified as nodes by their interaction in the functional network (h); n=6 per group. BPD: bronchopulmonary dysplasia; *Mmp10*: matrix metallopeptidase 10; *Ano3*: anoctamin 3; *Nmrk2*: nicotinamide riboside kinase 2; *Cxcl5*: C-X-C motif chemokine 5; *Ccl20*: CC-chemokine ligand 20; *IκBα*: nuclear factor of kappa light polypeptide gene enhancer in B-cells inhibitor, alpha; *Chodl*: chondrolectin; *Acta1*: actin alpha 1; *Ccl2*: CC-chemokine ligand 2; *Eda2r*: ectodysplasin A2 receptor; *Crabp1*: cellular retinoic acid-binding protein 1; *Glb1l3*: galactosidase beta 1 like 3; *Zfp663*: zinc finger protein 663; *Glp1r*: glucagon like peptide 1 receptor; *Havcr1*: hepatitis A virus cellular receptor 1; *Slc26a10*: solute carrier family 26 member 10; *Adcy8*: adenylate cyclase 8; *Abca17*: ATP-binding cassette, sub-family A (ABC1), member 17; *Cidec*: cell death inducing DFFA like effector C; *Vsnl1*: visinin like 1; IL-17: interleukin-17; GO: Gene Ontology; MAPK: mitogen-activated protein kinase; CCR: C-C motif chemokine receptor; *Cxcr4*: C-X-C motif chemokine receptor 4.

increased additional targets in lungs of newborn mice that are genes observed in M1-like polarisation encoding *Il6*, *Il17A* and *Mmp12* (figure 2d). In contrast, M2-like markers, *e.g. Il4*, *Il13* and *Arg1*, were not significantly different between the two groups (figure 2e). To assess gene expression and the effect of oxygen concentration at earlier developmental time points, we performed quantitative real-time PCR on M1- and M2-like markers at P3 and P7 in lungs of mice exposed either to 40% or 85% O_2. The gene expression analyses revealed a marked lung-intrinsic increase in *Il6* and *Mmp12* (M1-like markers), whereas the M2-like markers (*Il4* and *Arg1*) were reduced at P3 and P7 after 85% O_2 (supplementary figure S1a–d).

IL-6/STAT3 signalling in neonatal mouse lungs after hyperoxia is related to loss of epithelial cells and increased mesenchymal markers

Since *Il6* mRNA was almost 20-fold upregulated in lungs of newborn mice exposed to prolonged hyperoxia (85% O_2), we assessed lung IL-6/STAT3 signalling early after birth (P3, P7) and at P28. The significant increase of IL-6 mRNA at P3 and P7 was related to a marked activation of its downstream effector, STAT3, and expression of its target gene *Socs3* at P7. Exposure to lower concentrations of oxygen (40% O_2) induced phosphorylation of STAT3 (p=0.0556) and a significant expression of *Socs3* at P3 (supplementary figure S2). In order to investigate severe chronic lung injury after oxygen, we continued the experiments with 85% O_2. At P28, we found fivefold increased IL-6 protein, a significant activation of its downstream effector, STAT3, and a higher expression of suppressor of cytokine signalling 3 (SOCS3) after hyperoxia when compared to normoxia (figure 2f–h and supplementary figure S3). These pro-inflammatory findings were related to an almost fivefold increased expression of αsma, also known as *Acta2*, a mesenchymal marker expressed by smooth muscle cells and myofibroblasts (figure 2i), and a lower protein abundance of SFTPC and aquaporin 5 (AQP5), ATII and ATI markers, respectively (figure 2j, k).

Loss of IL-6 preserves alveolar formation in newborn mice after hyperoxia

We next tested if loss of *Il6* would protect the newborn mice from hyperoxia-induced lung injury and permit alveolar formation. Although hyperoxia simplified alveoli in the WT mice, as indicated by reduced radial alveolar count and increased mean linear intercept, these abnormalities were attenuated in the $Il6^{-/-}$ mice (figure 3a–c). Similarly, *Il6* deficiency protected newborn mice from the 50% increase of the alveolar surface area of single alveoli observed in WT mice, reflecting an ability to develop a greater overall gas exchange surface area (figure 3d).

Loss of IL-6 preserves elastic fibre assembly and lung compliance after hyperoxia

Hyperoxia disrupted elastin deposition in WT lungs, leading to a loss of elastin at the tips of the secondary septae and "brush-like" elastic fibres in the primary septae (figure 3e). In contrast, less disorganised elastic fibres were detected in the lungs of hyperoxia-exposed $Il6^{-/-}$ mice, and the localisation at the tips of the secondary septae appeared similar to that observed in the normoxia-exposed animals. The absolute elastic fibre content per defined area (μm^2) was unaltered by hyperoxia or IL-6 deficiency. Hyperoxia, however, significantly increased the relative elastic fibre content in WT but not $Il6^{-/-}$ mice (figure 3f, g). These changes in elastic fibre localisation may account for the protection of $Il6^{-/-}$ from reduced lung compliance after hyperoxia (figure 3h). We next analysed elastic fibre components and found an increase in *Col1a1*, *Fbn1* and *Fbln5* mRNA in $Il6^{-/-}$ lungs compared to WT (figure 3i–k). Moreover, deficiency of *Il6* was associated with a decrease in myofibroblasts in both normoxia and hyperoxia (figure 3l, m). Although

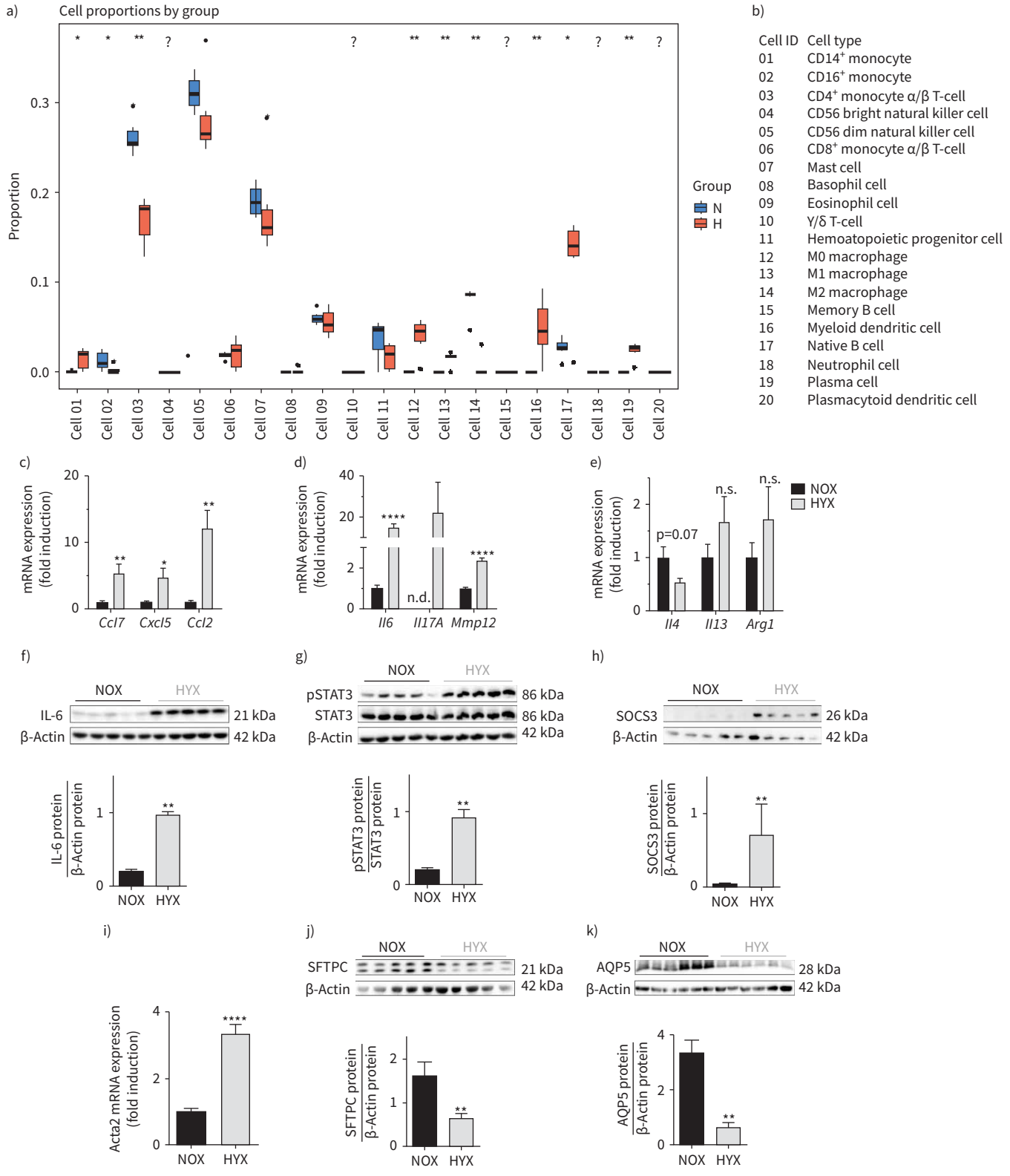

FIGURE 2 Prolonged hyperoxia activates macrophages and interleukin-6 (IL-6)/signal transducer and activator of transcription 3 (STAT3) signalling in neonatal lungs. a) Immune cell type proportions in lungs of newborn mice exposed to normoxia (N; 21% O_2) or hyperoxia (H; 80% O_2) for 14 days. Cell proportions were estimated by using the immunoStates *in silico* cell deconvolution (n=6 per group). b) List of identification numbers for each immune cell type. c–e) Newborn mice were exposed to normoxia (NOX; 21% O_2; black bars) or hyperoxia (HYX; 85% O_2; grey bars) for 28 days, followed by assessment of gene expression of chemokines identified as central nodes in the functional transcriptomic network and

regulating macrophage function using quantitative real-time PCR. c) CC-chemokine ligand 7 (*Ccl7*), C-X-C motif chemokine 5 (*Cxcl5*) and *Ccl2*. Measurement of mRNA expression of genes characteristic for M1-like polarisation. d) Interleukin 6 (*Il6*), *Il17A* and metalloproteinase 12 (*Mmp12*) and M2-like polarisation. e) *Il4*, *Il13* and arginase 1 (*Arg1*) using quantitative real-time PCR (n=6–7 per group). f) Measurement of IL-6 protein abundance by immunoblot in lungs of newborn mice exposed to normoxia (NOX; 21% O_2, black bars) or hyperoxia (HYX; 85% O_2, grey bars) from postnatal day 1 (P1) to P28 (n=5 per group); β-actin served as loading control; the densitometric analysis is shown below the immunoblot. g, h) Phosphorylated and total STAT3 (pSTAT3, STAT3; g) as well as SOCS3 protein (h) were assessed by immunoblot; densitometric summary data show pSTAT3 relative to total STAT3 and SOCS3 relative to β-actin, which served as loading control (n=5 per group). i) Measurement of α smooth muscle actin (αsma, known as *Acta2*) mRNA as a mesenchymal marker in lungs at P28 by quantitative real-time PCR (n=10–12 per group); gene expression is shown as fold induction. j, k) Immunoblots show epithelial cell markers at P28: surfactant protein C (SFTPC) as an indicator of alveolar epithelial type II cells (ATII) (j) and aquaporin 5 protein (AQP5) as a marker of ATI (k); β-actin served as loading control; the densitometric analysis is shown below the respective immunblot. Mean±SEM. Mann–Whitney test; *: p<0.05; **: p<0.01; ****: p<0.0001.

hyperoxia induced macrophage influx in both WT and $Il6^{-/-}$ mice, macrophage abundance was significantly lower in the hyperoxia-exposed $Il6^{-/-}$ mice than in WT (figure 3n, o).

Loss of IL-6 promotes surfactant protein expression and protects ATII after hyperoxia

Hyperoxia reduced *Sftpa* and *Sftpc* mRNA by almost 50% in WT mice, an effect that was completely blocked in the $Il6^{-/-}$ mice (figure 4a, b). In keeping with this finding, the protein abundance of SFTPC was significantly higher in hyperoxia-exposed $Il6^{-/-}$ mice compared to WT (figure 4c). Using immunofluorescent staining for SFTPC, we demonstrated that hyperoxia decreased the number of $SFTPC^+$ cells in both groups; however, $SFTPC^+$ cells were significantly higher in hyperoxia-exposed $Il6^{-/-}$ as compared to WT (figure 4d, e). Finally, using TUNEL staining we found that cell death, including ATII, was approximately 50% lower in the hyperoxia-exposed $Il6^{-/-}$ mice when compared to WT (figure 4f–h).

Pharmacological inhibition of global IL-6 signalling and IL-6 trans-signalling

We next treated newborn mice weekly, while exposed to hyperoxia, with injections of either IL-6 mAb sgp130Fc, or the respective vehicle [22] (figure 5a). While IL-6mAb globally neutralises IL-6, sgp130Fc only blocks the complex formed by IL-6 and sIL-6R, which is called IL-6 trans-signalling. Hyperoxia reduced survival of the newborn mice by ∼20%, but treatment with IL-6 mAb or sgp130Fc protected the mice (figure 5b). Both IL-6 mAb and sgp130Fc preserved alveolarisation in lungs exposed to prolonged hyperoxia (figure 5c–f), indicating that IL-6 trans-signalling *via* the sIL-6R was in part the underlying mechanism. Moreover, we found that mice treated with IL-6 mAb or sgp130Fc under hyperoxia were protected from loss of ATII, and had a similar number of ATII when compared to vehicle-treated mice under normoxia (figure 5g, h).

Hyperoxia activates macrophages via *loss of Klf4 and hyperoxia-exposed macrophages reduce cell survival of ATII*

Hyperoxia lowered the gene expression of the epithelial cell markers *Sftpc*, but not *Aqp5* in lung epithelial cells (MLE12) as indicators of ATII and ATI, respectively. Treatment of MLE12 with IL-6/sIL-6R had an additive effect on the reduction of *Sftpc*, but not *Aqp5* (figure 6a). To determine whether the secretome of macrophages (J774A1) regulates cell survival of MLE12, we exposed MLE12 cells to hyperoxia, followed by treatment with either standard cell medium (Co), normoxia-conditioned macrophage medium (CM^{NOX}) or hyperoxia-conditioned macrophage medium (CM^{HYX}). While the effect of CM^{NOX} was similar to Co, CM^{HYX} reduced proliferation of MLE12 (figure 6b). We next found that exposing macrophages (J774A.1) to hyperoxia for 24 and 48 h *in vitro* significantly increased IL-6 protein in the conditioned medium (figure 6c). In addition, we studied a possible mechanism by which hyperoxia activates M1-like polarisation. Prior reports have shown that loss of Klf4 promotes M1-like polarisation [23]. Indeed, hyperoxia reduced Klf4 protein in cultured macrophages by more than 50% (figure 6d). Furthermore, silencing of Klf4 in macrophages accentuated the expression of pro-inflammatory (M1-like) cytokines induced by hyperoxia (figure 6e). We next exposed primary murine macrophages (peritoneal) from WT mice to hyperoxia and found a significantly increased expression of *Mmp12* and *Tlr4* (M1-like) and a marked reduction of *Arg1* and *Fizz1* (M2-like) (figure 6f). Moreover, CM^{HYX} further decreased cell proliferation of MLE12 under hyperoxia when compared to CM^{NOX} (figure 6g). Finally, we exposed PCLS of 14-day-old mice to IL-6/sIL-6R and to normoxia or hyperoxia. IL-6 caused apoptosis in PCLS and had a significant additive effect on hyperoxia-induced apoptosis of $SFTPC^+$ cells (ATII) (figure 6h).

To translate our data to humans, we used hAECs (supplementary figure S4) and human monocyte-derived macrophages. Treatment of hAECs with IL-6/sIL-6R significantly reduced proliferation under normoxia

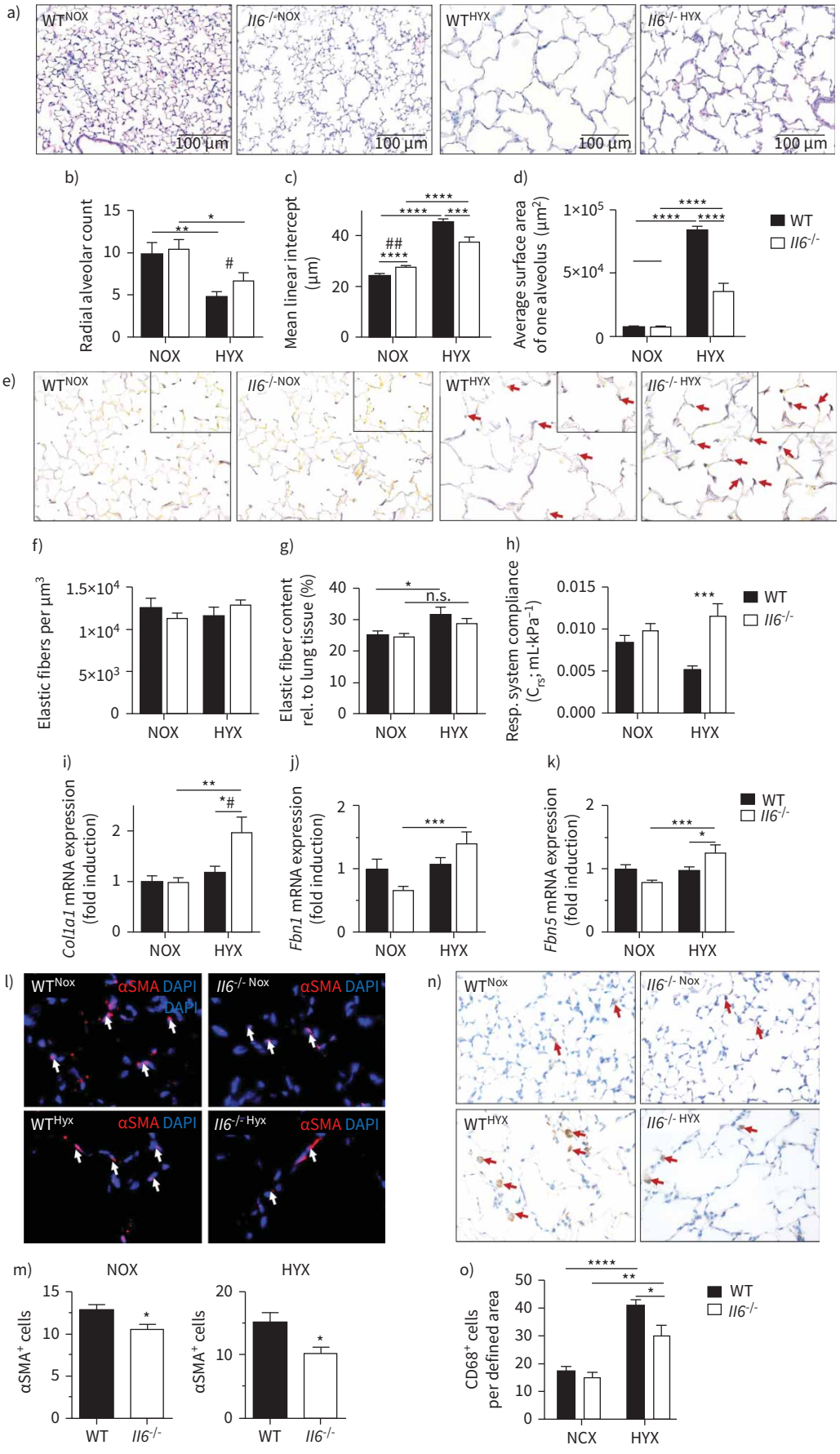
a)
WT^NOX
Il6^-/-NOX
WT^HYX
Il6^-/- HYX
100 µm
b)
Radial alveolar count
NOX
HYX
c)
Mean linear intercept (µm)
d)
Average surface area of one alveolus (µm²)
WT
Il6^-/-
e)
f)
Elastic fibers per µm³
g)
Elastic fiber content rel. to lung tissue (%)
n.s.
h)
Resp. system compliance (C_rs; mL·kPa⁻¹)
i)
Col1a1 mRNA expression (fold induction)
j)
Fbn1 mRNA expression (fold induction)
k)
Fbn5 mRNA expression (fold induction)
l)
WT^Nox
Il6^-/- Nox
WT^Hyx
Il6^-/- Hyx
αSMA DAPI
DAPI
m)
αSMA⁺ cells
n)
o)
CD68⁺ cells per defined area
NCX
HYX

FIGURE 3 Loss of interleukin 6 (*Il6*) preserves alveolar as well as elastic fibre formation, and reduces macrophage invasion in neonatal lungs after hyperoxia. a) Representative images of haematoxylin- and eosin-stained tissue sections showing alveolarisation in mice at postnatal day 28 (P28). Wildtype (WT) and *Il6* knockout mice ($Il6^{-/-}$) were exposed to hyperoxia (HYX; 85% O_2) or normoxia (NOX; 21% O_2) from postnatal day 1 (P1) to P28. b–d) Summary data of quantitative histomorphometric analyses: radial alveolar count (b), mean linear intercept (c), average surface area of one alveolus (d). e) Representative images of Hart's-stained tissue sections showing distribution and localisation of elastic fibres in mice at P28. Arrows indicate elastic fibres at the secondary tips after hyperoxia. f–g) Summary data of quantitative analyses of elastic fibres per defined area (μm^3) (f) and elastic fibre content relative (rel.) to lung tissue (%) (g). h) Measurement of respiratory (Resp.) system compliance using whole-body plethysmography in $Il6^{-/-}$ and WT mice at P28. i–k) Assessment of the expression of genes encoding components of lung matrix, including elastic fibres. i) Collagen 1α1 (*Col1a1*). j) Fibrillin 1 (*Fbn1*). k) Fibulin5 (*Fbln5*). l–m) Representative immunofluorescent staining of α-smooth muscle actin (αSMA) as a marker of myofibroblasts. White arrows depict positive stained cells (l); quantification data of αSMA^+ cells relative to all 4′,6-diamidino-2-phenylindole$^+$ ($DAPI^+$) cells (m). n–o) Representative images of macrophage using CD68 staining, ×100 magnification. Red arrows depict positive stained cells (n). Quantification data of $CD68^+$ cells per field of view (o). Mean±SEM; n=4–9 per group. Mann–Whitney test: $^{\#}$: p<0.05; $^{\#\#}$: p<0.01. Two-way ANOVA: *: p<0.05; **: p<0.01; ***: p<0.001; ****: p<0.0001; n.s.: not significant.

and hyperoxia for 24 h (figure 7a). We next exposed hAECs to standard cell medium (Co), to normoxia-conditioned human M1-like macrophage medium (hCM^{NOX}) or to hyperoxia-conditioned medium of human M1-like macrophages (hCM^{HYX}). Similar to the murine studies, we found that hCM^{HYX}, but not hCM^{NOX} further decreased proliferation of hAEC (figure 7b). Interestingly, CM^{HYX} of M0-like macrophages did not have an additive effect on hyperoxia-reduced proliferation of hAECs when compared to CM^{NOX} (supplementary figure S5). Finally, exposure of M1-like differentiated human monocyte-derived macrophages to hyperoxia for 48 h increased significantly the gene expression of human *IL6* (h*IL6*), *TNFa*, *TLR4* and *IL1b* (figure 7c).

Inflammatory serum biomarker profiling in premature infants for oxygen and BPD

Cytokine multiplex assay in plasma of preterm infants determined macrophage-related cytokines (regulated upon activation, normal T-cell expressed and presumably secreted (RANTES), monocyte-chemotactic protein 3 (MCP3), monokine-induced by gamma interferon (MIG)) and IL-6 (figure 8a) as potential biomarkers that identify infants receiving oxygen therapy at risk of developing BPD. By mixed linear modelling, infants that progressed to BPD demonstrated a longitudinal pattern of changes in plasma cytokine levels that differed from that seen in infants that did not develop BPD (figure 8b–e). Moreover, we performed a nonparametric fitted curve, followed by statistical analysis to determine the difference between BPD *versus* non-BPD at 32 weeks and 36 weeks (figure 8f). We found at 32 weeks in infants developing BPD increased concentrations of interleukin-1 receptor antagonist (IL1RA) (p=0.026), and a trend for increased intercellular adhesion molecule (ICAM) (CD54; p=0.075). These cytokines are either polarising or secreted by macrophages. At 36 weeks, we only detected a mild but not significant elevation of interferon gamma (p=0.16) and macrophage inflammatory protein α (CCL3; p=0.15), likely owing to small sample size. This will need to be verified through larger prospective longitudinal studies.

Immune ($CD45^+$ and $CD68^+$) cell influx with activation of IL-6/STAT3 signalling and reduced epithelial cells in lungs of infants with BPD

Finally, we analysed six postnatal human BPD lungs and six age-matched control lungs (table 1). CD45 immunofluorescent staining displayed a significant increase of immune cells in BPD lungs. Subsequent specific staining for CD45 and CD68, a marker of macrophages, showed significantly higher number of immune cells and macrophages in lungs with BPD when compared to non-BPD (figure 9a, b). *In situ* hybridisation of h*IL6* revealed higher number of h*IL6* mRNA-expressing cells in lungs with BPD when compared to the age-matched control lungs (figure 9c). The combination of *in situ* hybridisation of h*IL6* and CD68 immunofluorescent staining demonstrated significantly higher expression of h*IL6* in macrophages in lungs with BPD than in non-BPD (figure 9d). Immunofluorescent staining for STAT3 as downstream of IL-6, and CHD1 (epithelial cell marker) showed an activation of STAT3 and a reduction of $CDH1^+$ cells only in sex- and age-matched pairs (male), whereas infants matching for age, but not for sex (male *versus* female) did not show significant changes, indicating possible sex-specific differences (figure 9e–h). Finally, we stained for SFTPC as a marker of ATII and found an age-related association of number of ATII with BPD. The age of the infants with BPD significantly correlated with the decrease of ATII (R^2=0.5794; p=0.0062), whereas non-BPD showed a trend of increased ATII with age (figure 9i). In

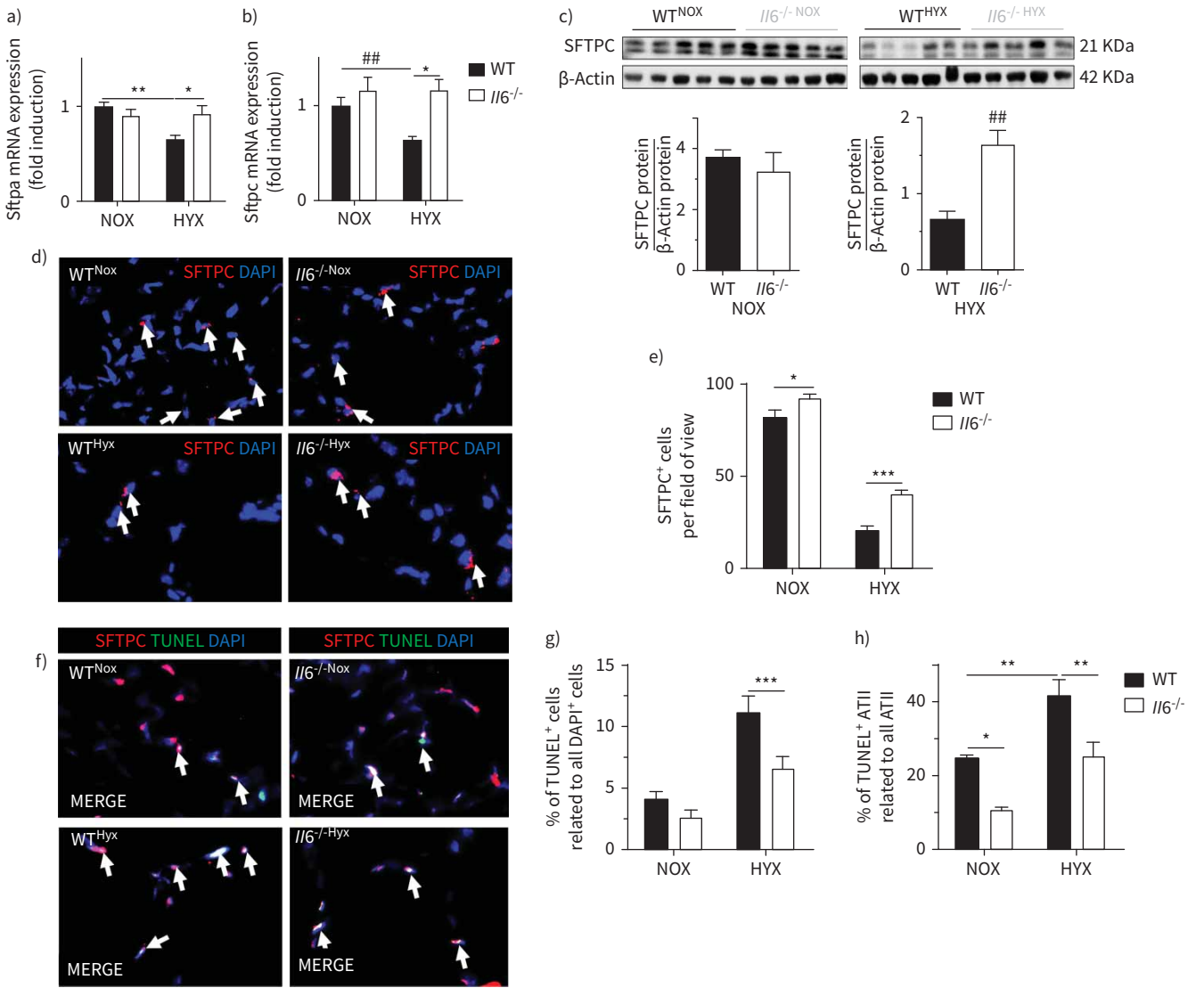

FIGURE 4 Loss of interleukin 6 (*Il6*) protects alveolar epithelial type II cells (ATII) in lungs of newborn mice after exposure to prolonged hyperoxia. Wildtype (WT) and *Il6* knockout mice ($Il6^{-/-}$) were exposed to hyperoxia (HYX; 85% O_2) or normoxia (NOX; 21% O_2) from postnatal day 1 (P1) to P28. a–b) Assessment of expression of genes encoding surfactant proteins (*Sftp*) in lungs at P28: *Sftpa* (a) and *Sftpc* (b). c) Immunoblot showing surfactant protein C (SFTPC) protein abundance in lungs at P28; SFTPC protein was related to β-actin, which served as loading control; densitometric data are displayed below the respective immunoblot. d) Representative immunofluorescence staining for surfactant protein C (SFTPC; red) as an indicator of ATII in lungs at P28; 4′,6-diamidino-2-phenylindole (DAPI) was used for nuclear staining, ×100 magnification. $SFTPC^+$ cells are indicated with white arrows. e) Quantitative data summary of $SFTPC^+$ cells per field of view. f–h) Representative co-immunofluorescence staining for terminal deoxynucleotidyl transferase dUTP nick end labelling (TUNEL) as an indicator of cell death (green) and SFTPC (red) in lungs at P28; DAPI was used for nuclear staining, ×100 magnification (f). Quantitative summary data of the percentage of $TUNEL^+$ cells (g), and $TUNEL^+$ ATII relative to all ATII (h). Mean±SEM; n=4–9 per group; Mann–Whitney test: ##: p<0.01 or as indicated; two-way ANOVA followed by Dunn's post test: *: p<0.05; **: p<0.01; ***: p<0.001.

summary, these data demonstrate that the pathogenesis of BPD is intimately linked to inflammation with macrophage-derived h*IL6*, STAT3 activation, and ultimately loss of epithelial cells and ATII over time.

Discussion

This study presents a novel mechanism by which hyperoxia adversely affects ATII homeostasis and elastic fibre formation *via* macrophage activation, resulting in enhanced activation of the IL-6 axis by IL-6 trans-signalling *via* sIL-6R, and ultimately inhibiting alveolar formation and impairing lung function. The data provide strong evidence that inhibition of IL-6 trans-signalling offers an innovative pharmacological target to enable lung growth in premature infants at risk for BPD. This novel inflammatory paradigm in the pathogenesis of BPD is

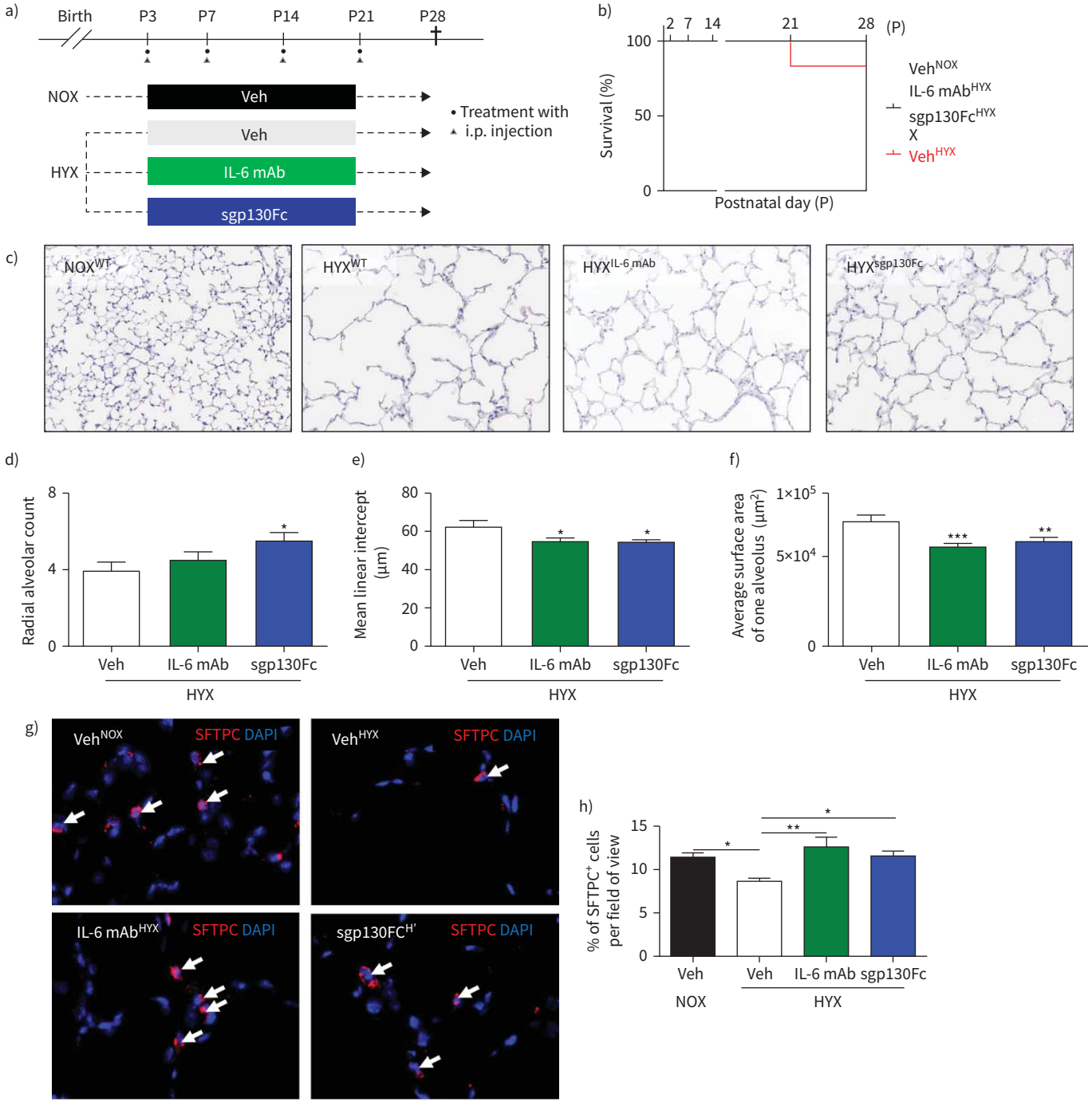

FIGURE 5 Inhibition of global interleukin 6 (IL-6) signalling and IL-6 trans-signalling enables lung growth and promotes ATII survival in lungs of newborn mice exposed to prolonged hyperoxia (HYX). a) Scheme of the experimental design. Wildtype (WT) mice were exposed to hyperoxia (85% O_2) from postnatal day 1 (P1) to P28; mice were treated intraperitoneally (*i.p.*) with vehicle (Veh), IL-6 mAb or sgp130Fc. b) Survival curve from birth until P28: vehicle-treated mice in normoxia (NOX); vehicle-treated mice in HYX; IL-6 mAb-treated mice in HYX; and sgp130Fc-treated mice in HYX. c) Representative images of haematoxylin- and eosin-stained tissue sections showing alveolarisation in mice at P28. d–f) Summary data of the quantitative histomorphometric analysis: radial alveolar count (d), mean linear intercept (e), and average surface area of one alveolus (f). g) Representative immunofluorescence staining for surfactant protein C (SFTPC; red) as an indicator of alveolar epithelial cells type II (ATII) in lungs at P28; 4′,6-diamidino-2-phenylindole (DAPI) was used for nuclear staining, ×100 magnification. $SFTPC^+$ cells are indicated with white arrows. h) Quantitative data summary of $SFTPC^+$ cells per field of view in %. Mean±SEM; n=4–6 per group. One-way Anova followed by Bonferroni's post-test: *: p<0.05; **: p<0.01; ***: p<0.001.

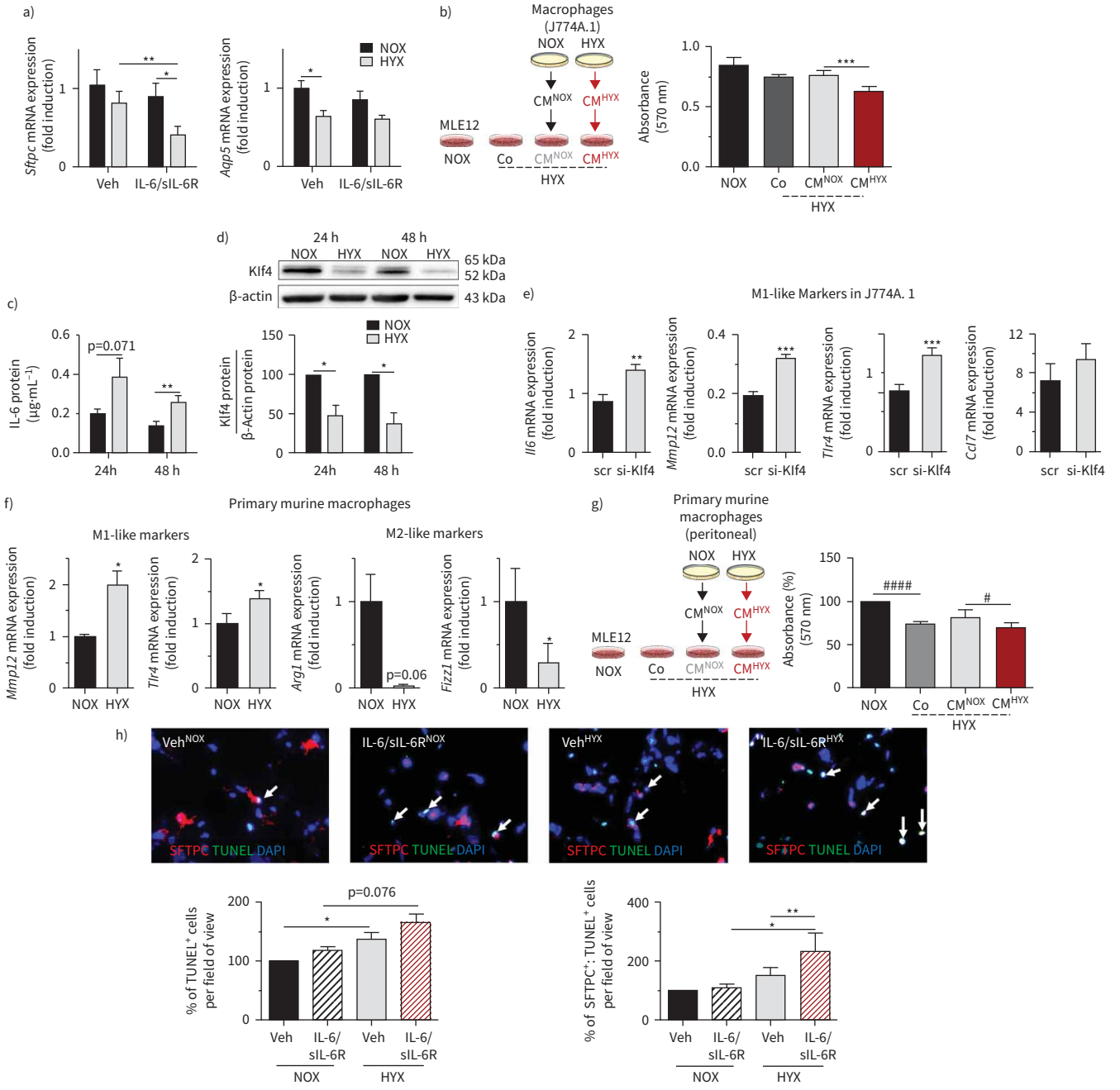

FIGURE 6 Hyperoxia-conditioned murine macrophages and interleukin 6 (IL-6)/soluble IL-6 receptor (sIL-6R) trigger hyperoxia-induced apoptosis of alveolar epithelial type II cells (ATII). a) Assessment of gene expression of surfactant protein C (*Sftpc*) and aquaporin 5 (*Aqp5*) in murine lung epithelial cells (MLE12). MLE12 were cultured in serum-rich medium, followed by serum-reduced medium for 12 h. Afterwards the cells were treated either with vehicle (Veh) or IL-6/sIL-6R and exposed to hyperoxia (HYX; 85% O_2) or normoxia (NOX; 21% O_2) for 24 h; n=11 per group; β-actin served as housekeeping gene. b) Scheme depicting the experimental design: macrophages (J774.A1) were exposed to NOX or HYX for 48 h; subsequently, MLE12 were exposed to HYX and treated with conditioned medium (CM) of NOX-exposed macrophages (CM^{NOX}), CM^{HYX} or Veh (untreated medium, Co) for 24 h; control MLE12 were exposed to NOX. At the end, proliferation of MLE12 was assessed using MTT assay; n=12–30 per group. c) Measurement of IL-6 protein using ELISA in supernatants of J744.A1 macrophages. J744.A1 were cultured in serum-rich medium, followed by exposure to HYX or NOX for 24 h and 48 h; n=8 per group. d) Immunoblot showing Krüppel-like factor 4 (Klf4) protein abundance in macrophages (J774.A1) after exposure to NOX or HYX for 24 h or 48 h; Klf4 protein was related to β-actin, which served as a loading control; densitometric data are displayed under the immunoblot; n=4–5 per group. e) Klf4 was suppressed in macrophages (J744.A1). Cells were transfected with small interfering RNA (siRNA) against Klf4 (si-klf4) or scrambled siRNA (scr) using the endo-porter technique, followed by a recovery time of 24 h in serum-rich medium. Subsequently, cells were starved with serum-reduced medium. Gene expression of macrophage markers was assessed after exposure to HYX for 48 h: *Il6*, metalloproteinase 12 (*Mmp12*), toll-like receptor 4 (*Tlr4*) and CC-chemokine ligand 7 (*Ccl7*); β-actin served as a

housekeeping gene; mean±SEM; n=4–5 per group. f) Primary murine macrophages (peritoneal) were isolated and cultured for 24 h in serum-rich medium. Subsequently, cells were exposed to NOX or HYX for 48 h in serum-reduced medium. Gene expression of M1-like (*Mmp12*, *Tlr4*) and M2-like (arginase 1 (*Arg1*), resistin-like molecule alpha 1 (*Fizz1*)) markers were assessed using quantitative real-time PCR; β-actin served as a housekeeping gene. g) Similar to (b), primary murine macrophages were exposed to NOX or HYX for 48 h; subsequently MLE12 were exposed to HYX and treated with CM^{NOX}, CM^{HYX} or Veh (untreated medium, Co) of primary murine macrophages; control MLE12 were exposed to NOX. After 24 h, proliferation of MLE12 was assessed using MTT assay; n=12–30 per group. h) Precision-cut lung slices of 14-day-old mice were treated either with Veh or IL-6/sIL-6R and exposed to NOX or HYX for 48 h; n=3–4 per group. Representative co-immunofluorescence staining for terminal deoxynucleotidyl transferase dUTP nick end labelling (TUNEL) as an indicator of apoptosis (green) and surfactant protein C (SFTPC) (ATII, red), ×100 magnification, along with quantitative summary data of the percentage of $TUNEL^+$ and $SFTPC^+$:$TUNEL^+$ cells relative to all ATII; mean±SEM. Paired t-test: *: p<0.05, **: p<0.01, ***: p<0.001; repeated measures. One-way ANOVA followed by Bonferroni's post-test: #: p<0.05, ####: p<0.0001. DAPI: 4′,6-diamidino-2-phenylindole.

based on *in vivo* studies using genetic modified mice with deletion of *Il6*, pharmacological treatment targeting global and IL-6 trans-signalling, and finally human studies using serum and lungs of infants with and without BPD along with hAEC and monocyte-derived macrophage cell culture studies.

Inflammation is a central mechanism in BPD [13]. Recent studies highlighted that resident alveolar macrophages are activated by hyperoxia, causing them to contribute to abnormal structural development of the immature mouse lung [15]. KALYMBETOVA *et al.* [15] show that hyperoxia causes a loss of resident alveolar macrophages in lungs of newborn mice, while a novel population of $CD45^+CD11c^+SiglecF^+CD11b^+CD68^+MHCII^+$cells emerges. The authors propose that residential alveolar macrophages transdifferentiate into this new population that contributes to arrested alveolarisation [15]. In

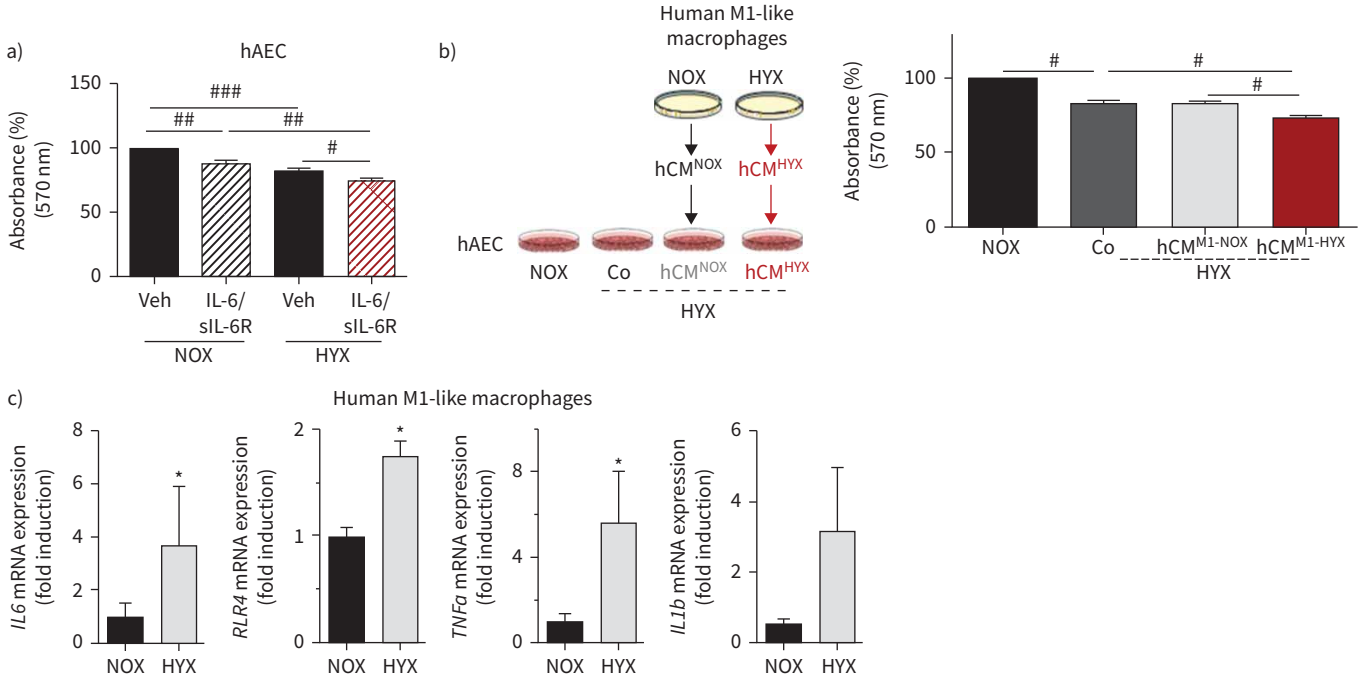

FIGURE 7 Interleukin 6 (IL-6)/soluble IL-6 receptor (sIL-6R) and human M1-like macrophages adversely affect human alveolar epithelial cell (hAEC) homeostasis. a) Proliferation of hAECs was assessed using MTT assay; hAECs were cultured in serum-rich medium for 24 h. Afterwards the cells were treated either with vehicle (Veh) or IL-6/sIL-6R and exposed to hyperoxia (HYX; 85% O_2) or normoxia (NOX; 21% O_2) for 24 h; n=6 per group. b) Scheme depicting the experimental design: human M1-like macrophages were exposed to NOX or HYX for 48 h and conditioned medium (CM) was collected; subsequently, hAECs were treated under HYX with CM of human NOX-exposed macrophages (hCM^{NOX}), hCM^{HYX} or vehicle (Co) for 24 h; control hAECs were exposed to NOX. At the end, proliferation of hAECs was assessed using MTT assay; n=4 per group. c) Human monocytes were isolated from blood and treated with granulocyte macrophage-colony stimulating factor (100 ng·mL^{-1}) in serum-rich medium and exposed to NOX or HYX for 48 h, followed by assessment of expression of genes encoding for macrophage markers (interleukin 6 (*IL6*), toll-like receptor 4 (*TLR4*), tumour necrosis factor alpha (*TNFα*) and interleukin1b (*IL1b*)) using quantitative real-time PCR; β-actin served as a housekeeping gene. Mean±SEM; n=4–5 per group. Repeated measures one-way ANOVA with Bonferroni's post-test: #: p<0.05; ##: p<0.01; ###: p<0.001; Wilcoxon paired t-test: *: p<0.05.

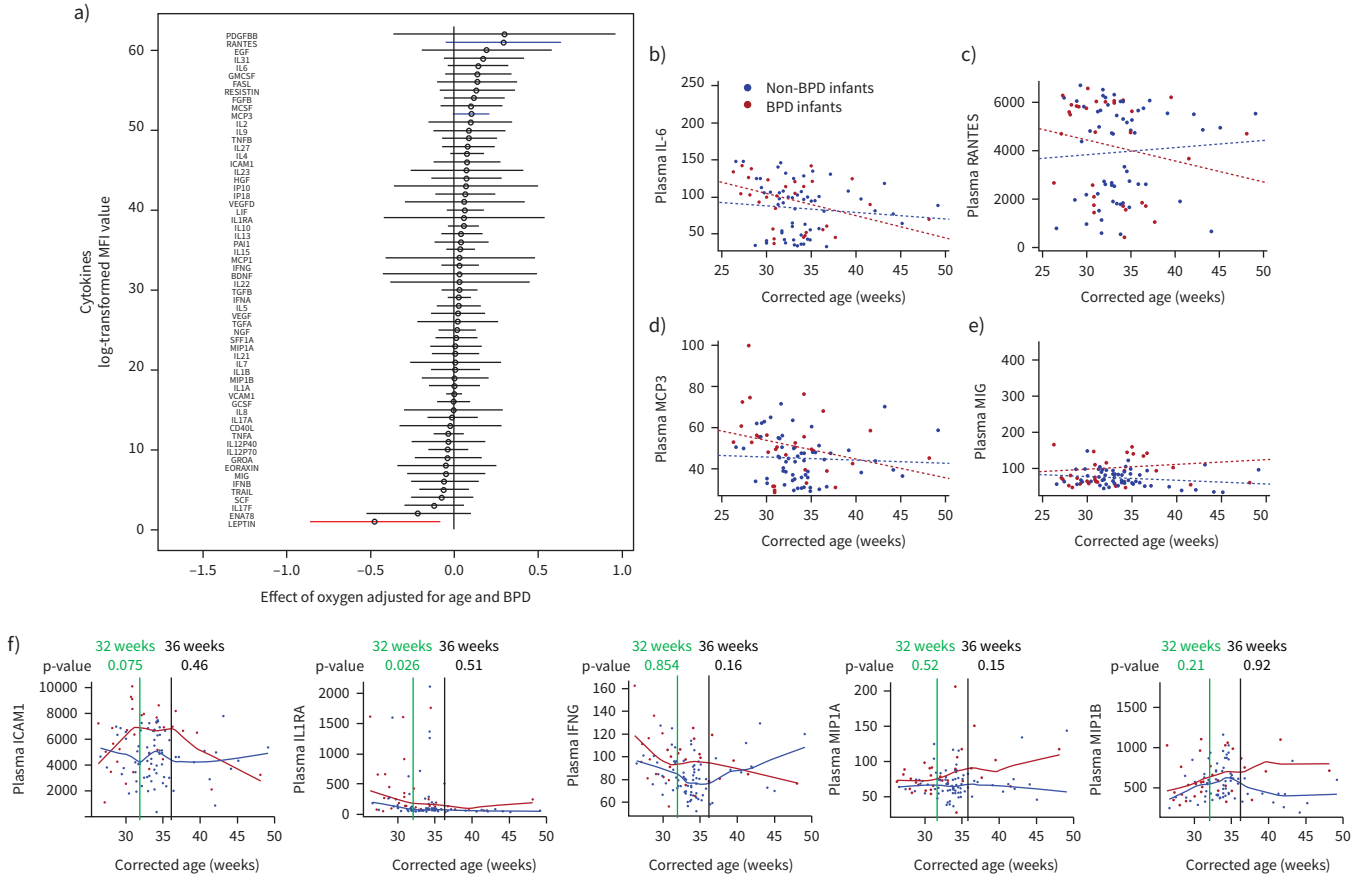

FIGURE 8 Clinical data showing the dynamic of cytokine concentrations in plasma of infants with and without bronchopulmonary dysplasia (BPD). a) Forest plot displaying the effect of oxygen on cystokine concentrations in premature infants (n=55). Data were adjusted for age and BPD. Plasma cytokines were measured using multiplex assay; blue and red lines highlight most upregulated and downregulated cytokines. MFI: mean fluorescence intensity. b–e) Mixed linear modelling to show a longitudinal pattern of changes in plasma cytokine levels in infants that progressed to BPD (red dots) *versus* non-BPD (blue dots). Plasma interleukin 6 (IL-6) (b); and macrophage related cytokines (c–e): regulated upon activation, normal T-cell expressed and presumably secreted (RANTES) (CCL5: CC-chemokine ligand 5) (c); monocyte-chemotactic protein 3 (MCP3) (CC-chemokine ligand 7, CCL7) (d); and monokine-induced by gamma interferon (MIG) (chemokine (C-X-C motif) ligand 9) (e). f) Nonparametric fitted curve for intercellular adhesion molecule 1 (ICAM; CD54), interleukin 1 receptor antagonist (IL1RA), interferon gamma (IFNG), macrophage inflammatory protein α (MIP1A; CCL3; p=0.15) and MIP1B (CCL4). Statistical differences between BPD and non-BPD infants were tested at 32 weeks (green line) and 36 weeks (black line). The respective p-values are indicated.

the present study, for the first time, we applied a comprehensive bioinformatics approach using *in silico* deconvolution of cell proportions from transcriptomic data in an experimental BPD model. We determined an immune cell proportion with reduction of the T-cell and increase in the B-cell population in lungs of mice exposed to prolonged hyperoxia. This is similar to a recent report showing a significant depletion of single positive $CD4^+$ as well as $CD8^+$ T-cells [24], and an increased proportion of naïve B-cells after hyperoxia [25]. Most striking, our data identified a reduction of M2-like macrophages, and an upregulation of M1-like macrophages that could possibly emerge from resident alveolar macrophages [15]. To further test this notion and to define the diverse macrophage phenotypes single-cell RNA sequencing over time should be performed.

Further analyses verified that chemokines regulating macrophage function are highly upregulated by hyperoxia, and that cytokine–cytokine receptor interaction and IL-17 signalling are the most affected pathways. Interestingly, IL-6 directs the immune response toward the Th17 phenotype, and IL-17 increases after hyperoxia in both alveolar macrophages and in lung epithelial cells [26, 27]. The role of IL-6 in neonatal lung injury, however, has been controversially discussed. While overexpression of IL-6 aggravated lung injury in newborn mice that were exposed to hyperoxia after birth, IL-6 overexpression provides protective effects against oxidant-mediated injury when mice are exposed to hyperoxia from day

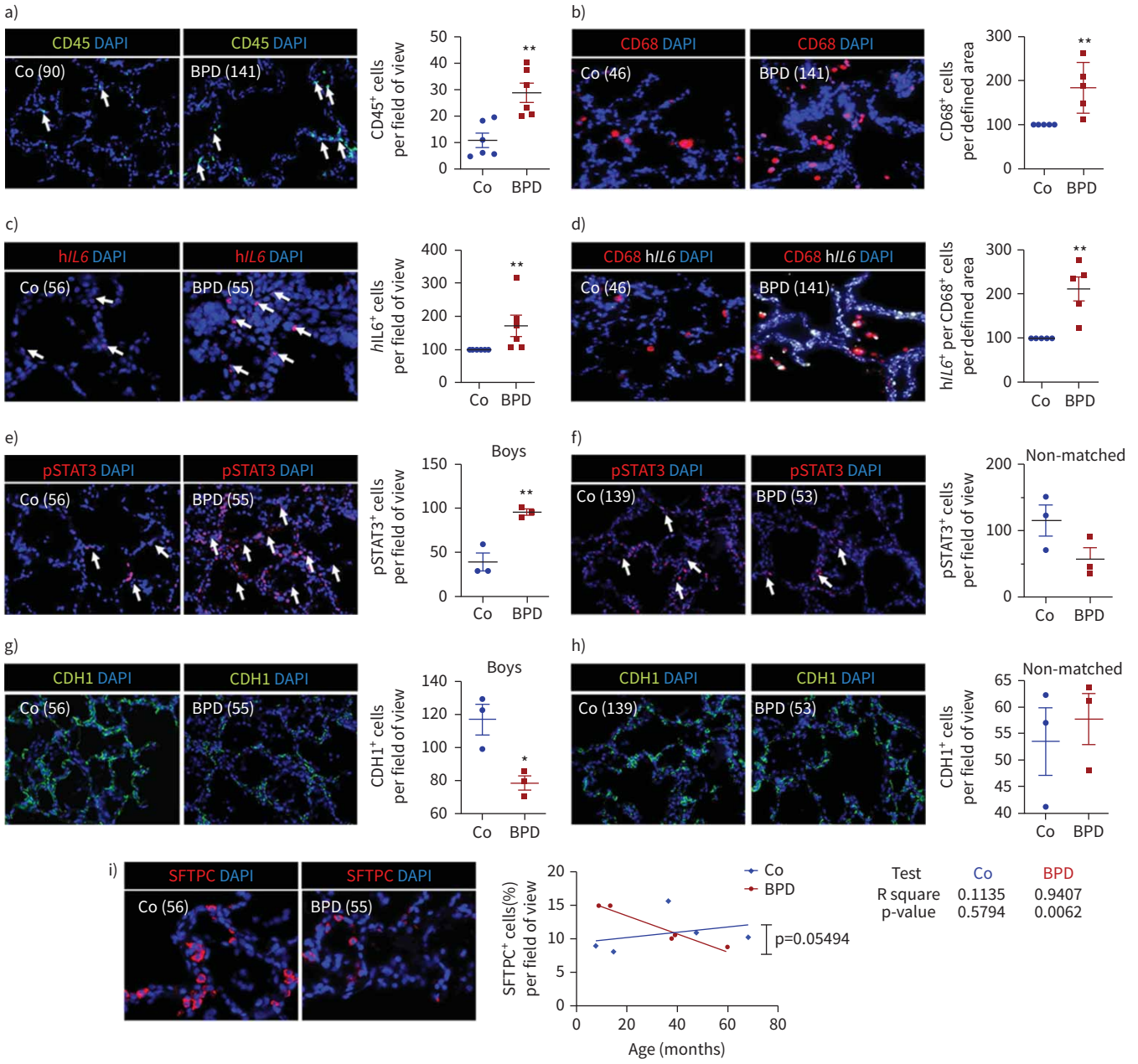

FIGURE 9 Inflammation and interleukin 6 (IL-6)/signal transducer and activator of transcription 3 (STAT3) signalling in lungs of infants with bronchopulmonary dysplasia (BPD) and non-BPD. a) Representative immunofluorescent staining for immune cells using CD45 as a marker (green) in age-matched BPD and control lungs (Co); the lung identification numbers of the infants are indicated in brackets. Immune cells (CD45$^+$ cells) were counted in 4–12 fields of view per lung. Summary data of the quantification of immune cells (CD45$^+$ cells) per field of view for all infants (n=6 per group). DAPI: 4′,6-diamidino-2-phenylindole. b) Representative co-immunofluorescent localisation of CD68 (marker of macrophages, red) in age-matched BPD and Co lungs; white arrows are indicating CD68$^+$ cells. The analysis of CD68$^+$ cells per 6–12 fields of view is shown next to the images; n=6 per group. c) Representative localisation of human *IL6* (h*IL6*, red) in lungs with BPD and Co; white arrows are indicating h*IL6*$^+$ *in situ* hybridisation. The analysis of h*IL6*$^+$ cells per 6–12 fields of view is shown next to the images; n=6 per group. d) Representative co-immunofluorescent localisation of CD68 (marker of macrophages, red) with h*IL6* (white; *in situ* hybridisation) in age-matched BPD and Co lungs; white arrows are indicating CD68$^+$ and h*Il6*$^+$. The analysis of h*IL6* mRNA expression per CD68$^+$ cells per 6–12 fields of view is shown next to the images; n=6 per group. e, f) Representative immunofluorescent staining showing pSTAT3 positive staining in lungs with BPD and Co; white arrows indicate pSTAT3$^+$ cells. The analysis of pSTAT3$^+$ cells in 4–12 fields of view was performed for sex- and age-matched BPD and control lungs (boys; n=3 per group) (e) as well as for age-matched, but not sex-matched BPD and control lungs (n=3 per group) (f). The graph is shown next to the respective images. g, h) Representative immunofluorescent staining showing CDH1 (green) positive staining in BPD and control lungs. The analysis of CDH1$^+$ cells in 4–12 fields of view was performed for sex- and age-matched BPD and Co lungs (boys; n=3 per group) (g) as well as for age-matched, but not sex-matched BPD and Co lungs (n=3 per group) (h). The graph is shown next to the respective images. i) Representative immunofluorescent of surfactant protein C (SFTPC; marker of

alveolar epithelial type II cells (ATII), red) in BPD and Co lungs. The analysis of linear regression for the amount of $SFTPC^+$ and age is shown in the graph (BPD, red; Co, blue); r^2 and p-value are indicated next to the graph; n=5 per group. Mean±SEM. Mann–Whitney test or t-test: *: p<0.05; **: p<0.01.

three to six of life [28, 29]. In contrast, the present study demonstrates that *Il6* null mice exhibit a mild reduction of alveoli already under normoxia that could be related to reduced number of myofibroblasts and possibly impaired secondary septation. While this notion is speculative and requires further investigation, our current findings along with prior studies highlight the importance of the tight regulation of IL-6 during discrete windows of lung development.

Various experimental models have been used to investigate the pathogenesis of BPD, including exposure to increased concentrations of oxygen, mechanical ventilation or infection [10, 30, 31]. When interpreting data, various criteria including sex, age, strain, injurious stimuli and duration of exposure have to be taken into account [32–34]. Reports demonstrated that the injury and the lung phenotype depend on the injurious stimuli and on the time of exposure. For example, continuous exposure to 40% O_2 from P1 until P4 or P14 adversely impacted alveolar formation and gas exchange surface, but not septal wall thickness as an indicator of matrix remodelling. On the contrary, only the severe BPD model with exposure of newborn mouse pups to 85% O_2 recapitulated both a marked impact on alveolarisation and on alveolar septal wall thickness [32, 35, 36]. In the present study, we used 85% O_2 for a prolonged period to induce a severe chronic lung injury with marked inflammation. Future studies, however, should include the impact of oxygen concentration and time of exposure in combination with mechanical ventilation and/or infection.

IL-6 is a multifunctional pro-inflammatory cytokine that regulates cell survival, differentiation of immune cells, such as macrophages, neutrophils as well as T-cells, and induces matrix remodelling that favours fibrosis [37, 38] as seen in chronic lung diseases [39]. Clinical studies showed increased concentrations of IL-6, sIL-6R and sgp130 in tracheal aspirates of infants evolving BPD [40–42]. ATII–macrophage interaction has been suggested by prior studies showing that alveolar epithelial IL-6-activated STAT3 signalling mediates inflammation, likely *via* macrophages [43]. We provide evidence *in vivo* and *in vitro* that hyperoxia disrupts macrophage–hAEC interaction by increasing various macrophage regulating cytokines, including *Il6*, inducing reduced survival of hAECs and promoting M1-like differentiation of macrophages [44, 45]. Since a previous study showed that the reduction of Klf4 favours M1-like polarisation, our present findings might be possibly related to a loss of Klf4 after hyperoxia [23]. Collectively, our data highlight the degree to which hyperoxia dysregulates the alveolar epithelial macrophage niche, but also the key role of IL-6 in orchestrating this cellular crosstalk. Recent reports suggest that targeting IL-6 signalling prevents emphysema-like disease [46] and may be a new therapeutic target for pulmonary arterial hypertension [47]. Here, we provide evidence that loss of IL-6 and pharmacological inhibition of IL-6 classic- and trans-signalling enables alveolar growth and lung function by protecting ATII survival and preserving distribution of elastic fibres in lungs of newborn mice after hyperoxia. Recent studies indicated that inhibition of proteolytic activity in mechanically ventilated newborn mice using the serine elastase inhibitor elafin enabled lung growth and reduced inflammation [21, 30]. The key role of protease and anti-protease balance in neonatal lung growth was further supported by the finding that infants evolving BPD have increased serum elastase concentrations [30]. Interestingly, proteases (*e.g.*, ADAM10 or ADAM17) have been described to act as a sheddase for the IL-6 receptor and a regulator of IL-6 signalling [48–50]. Thus, blocking of proteolytic activity could have an anti-inflammatory effect by preventing IL-6 signalling.

Inflammatory response and dysregulation of cytokines is a prominent feature of BPD. Increased number of immune cells in BPD is associated with decreased septation and fewer alveoli [12, 13, 15]. In the present study, we determined increased concentrations of plasma cytokines regulating macrophage recruitment and function, such as RANTES or MCP3, highlighting the systemic inflammatory response in BPD. Similarly, we found an upregulation of IL1RA and ICAM1, both cytokines regulating macrophage polarisation [51, 52]. Interestingly, serum ICAM level has been recently reported as a potential biomarker for BPD and was correlated with its severity [53]. Plasma IL-6 concentration was dynamically regulated with an early postnatal elevation of IL-6 by trend in infants developing BPD when compared to non-BPD. Since plasma does not necessarily reflect lung-intrinsic IL-6, tracheal aspirates might be more appropriate as shown in prior studies with increased IL-6 in infants with BPD [42]. However, the time point of measurement in the infant might not developmentally match our mouse model. The plasma cytokine pattern in infants with BPD was related to a significant increase of immune cells, specifically macrophages ($CD68^+$), and increased macrophage-derived *Il6* in lungs of infants with BPD, independent of sex and age. We linked this immune response to an activation of STAT3 signalling and loss of epithelial cells in male infants.

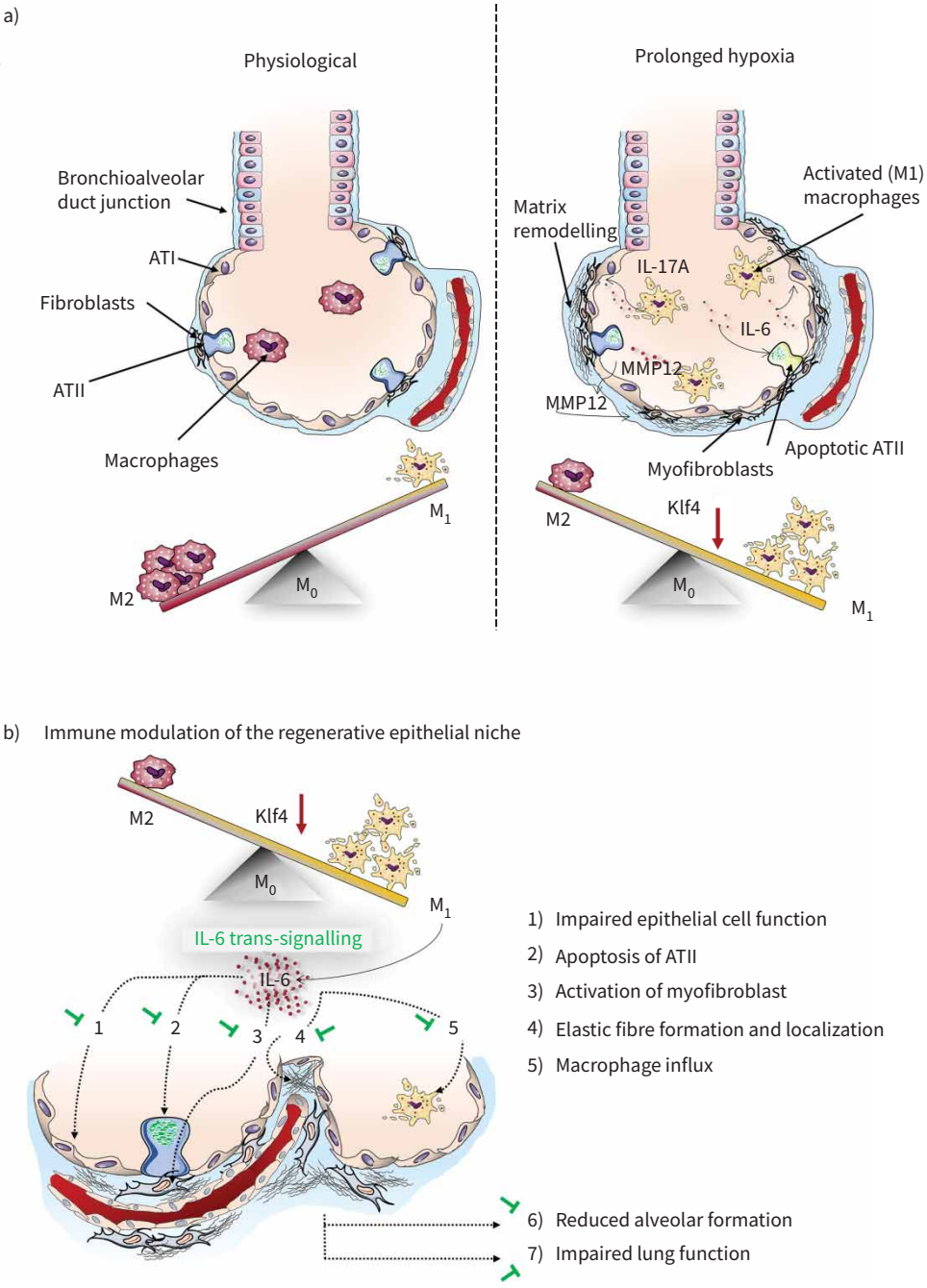

FIGURE 10 Proposed working model illustrating how hyperoxia induces macrophage polarisation. a) The M1-like-driven inflammatory phenotype leads to the secretion of cytokines, such as interleukin 6 (IL-6) and IL-17A, as well macrophage elastase, also known was metalloproteinase 12 (MMP12). This inflammatory alveolar microenvironment reduces survival of alveolar epithelial type II cells (ATII), whereas fibroblasts are activated and matrix remodelling is promoted. ATI: alveolar epithelial type I cell; Klf4: Krüppel-like factor 4. b) Polarisation of macrophages following hyperoxia leads to a release of IL-6, which adversely affects the regenerative epithelial niche. However, IL-6 deficiency protects from these changes by 1) promoting expression of surfactant proteins and 2) survival of ATII, 3) reducing myofibroblasts, 4) protecting from perturbed elastic fibre assembly and localisation, and 5) attenuating macrophage influx. These beneficial effects of IL-6 deficiency on the alveolar compartment enables 6) alveolar formation and 7) protects from reduced lung function, offering a new therapeutic target to treat BPD.

Interestingly, these effects were not evident in age-matched, but not sex-matched, BPD and non-BPD infants, suggesting a possible sex-specific IL-6/STAT3 response, which could contribute to sex-dependent differences in BPD [54]. Finally, we showed a correlation between age and the reduction of ATII in lungs with BPD, but not in non-BPD. Taken together our studies, in concert with prior studies, suggest that IL-6 as a macrophage-regulating cytokine, might serve as a useful biomarker of lung injury in very premature infants, and help to define the risk for BPD.

As depicted in our working model (figure 10), inflammation and damage of the regenerative epithelial niche by loss of ATII impairs alveolar formation and leads to emphysematous lung structure beyond infancy. The present study demonstrates that hyperoxia disrupts macrophage-ATII interaction by triggering IL-6/STAT3 signalling in murine and human lungs, but also identifies IL-6 as a potential early onset biomarker and sgp130Fc as a novel therapeutic strategy for infants at risk for BPD. The specific blockade of IL-6 trans-signalling predominantly inhibits the pro-inflammatory activities of IL-6 while the protective and regenerative function is not affected. This innovative therapeutic strategy is already in phase II clinical trial in patients with autoimmune disease [55] and offers new avenues for the treatment of BPD.

Acknowledgements: We greatly appreciate and thank Marlene Rabinovitch and Richard Bland (Dept of Pediatrics, and Cardiovascular Institute, and The Vera Moulton Wall Center for Pulmonary Vascular Disease, Stanford University School of Medicine, Stanford) for their helpful suggestions. We thank the imaging facility of the Cologne Excellence Cluster on Cellular Stress Responses in Aging-Associated Diseases (CECAD) for their technical support. We also thank Sebahattin Cirak (Dept of Pediatrics, Center for Molecular Medicine Cologne, and Center for Rare Diseases Cologne, University of Cologne, University Hospital of Cologne, Cologne, Germany) and Ugur Akpulat (Dept of Pediatrics, Center for Molecular Medicine Cologne, University of Cologne, University Hospital of Cologne, Cologne, Germany; and University of Kastamonu, Turkey) for their technical support in cell culture studies. The IL-6mAb and sgp130Fc was kindly provided by Stefan Rose-John (Institute of Biochemistry, Christian-Albrechts-University Kiel, Germany).

Author contributions: D. Hirani, C.M. Alvira, S. Danopoulos, C. Milla, D. Al Alam, V. Barbarino, C. Pallasch, S. Rose John, M. Odenthal, G.S. Pryhuber, R. Savai and M.A. Alejandre Alcazar conceived and designed research; D. Hirani, C.M. Alvira, S. Danopoulos, M. Donato, C. Milla, K. Dinger, C. Vohlen, J. Mohr, V. Barbarino, S. Mansouri and M.A. Alejandre Alcazar performed experiments; D. Hirani, C.M. Alvira, S. Danopoulos, M. Donato, C. Milla, L. Tian, C. Vohlen, D. Al Alam and M.A. Alejandre Alcazar analysed data; D. Hirani, C.M. Alvira, S. Danopoulos, M. Donato, C. Milla, L. Tian, J. Selle, S. v. Koningsbruggen-Rietschel, J. Mohr, P. Khatri, D. Al Alam, J. Dötsch and M.A. Alejandre Alcazar interpreted results of experiments; D. Hirani, S. Danopoulos, M. Donato, J. Selle and M.A. Alejandre Alcazar prepared figures; D. Hirani and M.A. Alejandre Alcazar drafted manuscript; D. Hirani, C.M. Alvira, S. Danopoulos, C. Milla, D. Al Alam, J. Selle, W. Seeger and M.A. Alejandre Alcazar edited and revised manuscript; D. Hirani, C.M. Alvira, S. Danopoulos, M. Donato, C. Milla, L. Tian, J. Mohr, K. Dinger, C. Vohlen, J. Selle, S. v. Koningsbruggen-Rietschel, V. Barbarino, C. Pallasch, S. Rose John, M. Odenthal, G.S. Pryhuber, R. Savai, S. Mansouri, W. Seeger, P. Khatri, D. Al Alam, J. Dötsch and M.A. Alejandre Alcazar approved final version of manuscript.

Conflict of interest: D. Hirani has nothing to disclose. C.M. Alvira has nothing to disclose. S. Danopoulos has nothing to disclose. C. Milla reports grants from Proteostasis Inc and Eloxx Pharmaceuticals, grants and personal fees for advisory board work from Vertex Pharmaceuticals, outside the submitted work. M. Donato has nothing to disclose. L. Tian has nothing to disclose. J. Mohr has nothing to disclose. K. Dinger has nothing to disclose. C. Vohlen has nothing to disclose. J. Selle has nothing to disclose. S. v. Koningsbruggen-Rietschel has nothing to disclose. V. Barbarino has nothing to disclose. C. Pallasch has nothing to disclose. S. Rose John has nothing to disclose. M. Odenthal has nothing to disclose. G.S. Pryhuber reports grants from NHLBI, during the conduct of the study. S. Mansouri has nothing to disclose. R. Savai has nothing to disclose. W. Seeger reports personal fees from Actelion, Abivax, Bayer AG, Vectura, Medspray, United Therapeutics, Liquidia and Pieris, outside the submitted work. P. Khatri has nothing to disclose. D. Al Alam has nothing to disclose. J. Dötsch has nothing to disclose. M.A. Alejandre Alcazar has nothing to disclose.

Support statement: This work was supported by Deutsche Forschungsgemeinschaft (1636/2-1; M.A. Alejandre Alcazar), Marga und Walter Boll Stiftung (M.A. Alejandre Alcazar); Center for Molecular Medicine Cologne (M.A. Alejandre Alcazar), and University Hospital Cologne; Stanford Child Health Research Institute Tashia and John Morgridge Faculty Scholar Award (C.M. Alvira); the NIH HL122918 (C.M. Alvira), NIH R01HL141856 (D. Al Alam), NIH PO1HL108797-5974 Biomarker Core (C. Milla); NHLBI LungMAP Research Center. U01HL122681 (S. Danopoulos, D. Al Alam), Biorepository (1U01HL122700, G.S. Pryhuber) and Data Coordinating Center (1U01HL122638, G.S. Pryhuber). Funding information for this article has been deposited with the Crossref Funder Registry.

References

1 Northway WH, Jr, Rosan RC, Porter DY. Pulmonary disease following respirator therapy of hyaline-membrane disease. Bronchopulmonary dysplasia. *N Engl J Med* 1967; 276: 357–368.
2 Caskey S, Gough A, Rowan S, *et al.* Structural and functional lung impairment in adult survivors of bronchopulmonary dysplasia. *Ann Am Thorac Soc* 2016; 13: 1262–1270.
3 Thebaud B, Abman SH. Bronchopulmonary dysplasia: where have all the vessels gone? Roles of angiogenic growth factors in chronic lung disease. *Am J Respir Crit Care Med* 2007; 175: 978–985.
4 Hou A, Fu J, Yang H, *et al.* Hyperoxia stimulates the transdifferentiation of type II alveolar epithelial cells in newborn rats. *Am J Physiol Lung Cell Mol Physiol* 2015; 308: L861–L872.
5 Yee M, Buczynski BW, O'Reilly MA. Neonatal hyperoxia stimulates the expansion of alveolar epithelial type II cells. *Am J Respir Cell Mol Biol* 2014; 50: 757–766.
6 Rackley CR, Stripp BR. Building and maintaining the epithelium of the lung. *J Clin Invest* 2012; 122: 2724–2730.
7 Vaughan AE, Chapman HA. Failure of alveolar type 2 cell maintenance links neonatal distress with adult lung disease. *Am J Respir Cell Mol Biol* 2017; 56: 415–416.
8 Yee M, Domm W, Gelein R, *et al.* Alternative progenitor lineages regenerate the adult lung depleted of alveolar epithelial type 2 cells. *Am J Respir Cell Mol Biol* 2017; 56: 453–464.
9 Vyas-Read S, Wang W, Kato S, *et al.* Hyperoxia induces alveolar epithelial-to-mesenchymal cell transition. *Am J Physiol Lung Cell Mol Physiol* 2014; 306: L326–L340.
10 Alejandre-Alcazar MA, Kwapiszewska G, Reiss I, *et al.* Hyperoxia modulates TGF-beta/BMP signaling in a mouse model of bronchopulmonary dysplasia. *Am J Physiol Lung Cell Mol Physiol* 2007; 292: L537–L549.
11 Maloney JP, Gao L. Proinflammatory cytokines increase vascular endothelial growth factor expression in alveolar epithelial cells. *Mediators Inflamm* 2015; 2015: 387842.
12 Bhandari V, Choo-Wing R, Lee CG, *et al.* Hyperoxia causes angiopoietin 2-mediated acute lung injury and necrotic cell death. *Nat Med* 2006; 12: 1286–1293.
13 Liao J, Kapadia VS, Brown LS, *et al.* The NLRP3 inflammasome is critically involved in the development of bronchopulmonary dysplasia. *Nat Commun* 2015; 6: 8977.
14 Wolf J, Rose-John S, Garbers C. Interleukin-6 and its receptors: a highly regulated and dynamic system. *Cytokine* 2014; 70: 11–20.
15 Kalymbetova TV, Selvakumar B, Rodriguez-Castillo JA, *et al.* Resident alveolar macrophages are master regulators of arrested alveolarization in experimental bronchopulmonary dysplasia. *J Pathol* 2018; 245: 153–159.
16 Nold MF, Mangan NE, Rudloff I, *et al.* Interleukin-1 receptor antagonist prevents murine bronchopulmonary dysplasia induced by perinatal inflammation and hyperoxia. *Proc Natl Acad Sci USA* 2013; 110: 14384–14389.
17 Rudloff I, Cho SX, Bui CB, *et al.* Refining anti-inflammatory therapy strategies for bronchopulmonary dysplasia. *J Cell Mol Med* 2017; 21: 1128–1138.
18 Mohr J, Voggel J, Vohlen C, *et al.* IL-6/Smad2 signaling mediates acute kidney injury and regeneration in a murine model of neonatal hyperoxia. *FASEB J* 2019; 33: 5887–5902.
19 Szklarczyk D, Gable AL, Lyon D, *et al.* STRING v11: protein-protein association networks with increased coverage, supporting functional discovery in genome-wide experimental datasets. *Nucleic Acids Res* 2019; 47: D607–D613.
20 Vallania F, Tam A, Lofgren S, *et al.* Leveraging heterogeneity across multiple datasets increases cell-mixture deconvolution accuracy and reduces biological and technical biases. *Nat Commun* 2018; 9: 4735.
21 Hilgendorff A, Parai K, Ertsey R, *et al.* Inhibiting lung elastase activity enables lung growth in mechanically ventilated newborn mice. *Am J Respir Crit Care Med* 2011; 184: 537–546.
22 Ruwanpura SM, McLeod L, Dousha LF, *et al.* Therapeutic targeting of the IL-6 trans-signaling/mechanistic target of rapamycin complex 1 axis in pulmonary emphysema. *Am J Respir Crit Care Med* 2016; 194: 1494–1505.
23 Liao X, Sharma N, Kapadia F, *et al.* Kruppel-like factor 4 regulates macrophage polarization. *J Clin Invest* 2011; 121: 2736–2749.
24 Angusamy S, Mansour T, Abdulmageed M, *et al.* Altered thymocyte and T cell development in neonatal mice with hyperoxia-induced lung injury. *J Perinat Med* 2018; 46: 441–449.
25 Wang J, Chen Q, Corne J, *et al.* Pulmonary expression of leukemia inhibitory factor induces B cell hyperplasia and confers protection in hyperoxia. *J Biol Chem* 2003; 278: 31226–31232.
26 Nagato AC, Bezerra FS, Talvani A, *et al.* Hyperoxia promotes polarization of the immune response in ovalbumin-induced airway inflammation, leading to a TH17 cell phenotype. *Immun Inflamm Dis* 2015; 3: 321–337.
27 Varelias A, Gartlan KH, Kreijveld E, *et al.* Lung parenchyma-derived IL-6 promotes IL-17A-dependent acute lung injury after allogeneic stem cell transplantation. *Blood* 2015; 125: 2435–2444.
28 Choo-Wing R, Nedrelow JH, Homer RJ, *et al.* Developmental differences in the responses of IL-6 and IL-13 transgenic mice exposed to hyperoxia. *Am J Physiol Lung Cell Mol Physiol* 2007; 293: L142–L150.

29 Chetty A, Cao GJ, Manzo N, *et al.* The role of IL-6 and IL-11 in hyperoxic injury in developing lung. *Pediatr Pulmonol* 2008; 43: 297–304.
30 Alejandre Alcazar MA, Kaschwich M, Ertsey R, *et al.* Elafin treatment rescues EGFR-Klf4 signaling and lung cell survival in ventilated newborn mice. *Am J Respir Cell Mol Biol* 2018; 59: 623–634.
31 Shrestha AK, Bettini ML, Menon RT, *et al.* Consequences of early postnatal lipopolysaccharide exposure on developing lungs in mice. *Am J Physiol Lung Cell Mol Physiol* 2019; 316: L229–L244.
32 Leary S, Das P, Ponnalagu D, *et al.* Genetic strain and sex differences in a hyperoxia-induced mouse model of varying severity of bronchopulmonary dysplasia. *Am J Pathol* 2019; 189: 999–1014.
33 Tiono J, Surate Solaligue DE, Mizikova I, *et al.* Mouse genetic background impacts susceptibility to hyperoxia-driven perturbations to lung maturation. *Pediatr Pulmonol* 2019; 54: 1060–1077.
34 Will JP, Hirani DV, Thielen F, *et al.* Strain-dependent effects on lung structure, matrix remodeling and Stat3/Smad2 signaling in C57BL/6N and C57BL/6J mice after neonatal hyperoxia. *Am J Physiol Regul Integr Comp Physiol* 2019; 317: R169–R181.
35 Nardiello C, Mizikova I, Silva DM, *et al.* Standardisation of oxygen exposure in the development of mouse models for bronchopulmonary dysplasia. *Dis Model Mech* 2017; 10: 185–196.
36 Yee M, Chess PR, McGrath-Morrow SA, *et al.* Neonatal oxygen adversely affects lung function in adult mice without altering surfactant composition or activity. *Am J Physiol Lung Cell Mol Physiol* 2009; 297: L641–L649.
37 Fielding CA, Jones GW, McLoughlin RM, *et al.* Interleukin-6 signaling drives fibrosis in unresolved inflammation. *Immunity* 2014; 40: 40–50.
38 Le TT, Karmouty-Quintana H, Melicoff E, *et al.* Blockade of IL-6 trans signaling attenuates pulmonary fibrosis. *J Immunol* 2014; 193: 3755–3768.
39 Papiris SA, Tomos IP, Karakatsani A, *et al.* High levels of IL-6 and IL-8 characterize early-on idiopathic pulmonary fibrosis acute exacerbations. *Cytokine* 2018; 102: 168–172.
40 Chakraborty M, McGreal EP, Davies PL, *et al.* Role of interleukin-6, its receptor and soluble gp130 in chronic lung disease of prematurity. *Neonatology* 2013; 104: 161–167.
41 von Bismarck P, Claass A, Schickor C, *et al.* Altered pulmonary interleukin-6 signaling in preterm infants developing bronchopulmonary dysplasia. *Exp Lung Res* 2008; 34: 694–706.
42 Hsiao CC, Chang JC, Tsao LY, *et al.* Correlates of elevated interleukin-6 and 8-hydroxy-2'-deoxyguanosine levels in tracheal aspirates from very low birth weight infants who develop bronchopulmonary dysplasia. *Pediatr Neonatol* 2017; 58: 63–69.
43 Quinton LJ, Jones MR, Robson BE, *et al.* Alveolar epithelial STAT3, IL-6 family cytokines, and host defense during *Escherichia coli* pneumonia. *Am J Respir Cell Mol Biol* 2008; 38: 699–706.
44 Chuquimia OD, Petursdottir DH, Periolo N, *et al.* Alveolar epithelial cells are critical in protection of the respiratory tract by secretion of factors able to modulate the activity of pulmonary macrophages and directly control bacterial growth. *Infect Immun* 2013; 81: 381–389.
45 Thorley AJ, Ford PA, Giembycz MA, *et al.* Differential regulation of cytokine release and leukocyte migration by lipopolysaccharide-stimulated primary human lung alveolar type II epithelial cells and macrophages. *J Immunol* 2007; 178: 463–473.
46 Petrache I, Serban K. Lost in trans-IL-6 signaling: alveolar type II cell death in emphysema. *Am J Respir Crit Care Med* 2016; 194: 1441–1443.
47 Pullamsetti SS, Seeger W, Savai R. Classical IL-6 signaling: a promising therapeutic target for pulmonary arterial hypertension. *J Clin Invest* 2018; 128: 1720–1723.
48 Schumacher N, Meyer D, Mauermann A, *et al.* Shedding of endogenous interleukin-6 receptor (IL-6R) is governed by A disintegrin and metalloproteinase (ADAM) proteases while a full-length IL-6R isoform localizes to circulating microvesicles. *J Biol Chem* 2015; 290: 26059–26071.
49 Mullberg J, Schooltink H, Stoyan T, *et al.* The soluble interleukin-6 receptor is generated by shedding. *Eur J Immunol* 1993; 23: 473–480.
50 Matthews V, Schuster B, Schutze S, *et al.* Cellular cholesterol depletion triggers shedding of the human interleukin-6 receptor by ADAM10 and ADAM17 (TACE). *J Biol Chem* 2003; 278: 38829–38839.
51 Luz-Crawford P, Djouad F, Toupet K, *et al.* Mesenchymal stem cell-derived interleukin 1 receptor antagonist promotes macrophage polarization and inhibits B cell differentiation. *Stem Cells* 2016; 34: 483–492.
52 Gu W, Yao L, Li L, *et al.* ICAM-1 regulates macrophage polarization by suppressing MCP-1 expression *via* miR-124 upregulation. *Oncotarget* 2017; 8: 111882–111901.
53 Sahni M, Yeboah B, Das P, *et al.* Novel biomarkers of bronchopulmonary dysplasia and bronchopulmonary dysplasia-associated pulmonary hypertension. *J Perinatol* 2020; 40: 1634–1643.
54 Mansson J, Fellman V, Stjernqvist K, *et al.* Extremely preterm birth affects boys more and socio-economic and neonatal variables pose sex-specific risks. *Acta Paediatr* 2015; 104: 514–521.
55 Garbers C, Heink S, Korn T, *et al.* Interleukin-6: designing specific therapeutics for a complex cytokine. *Nat Rev Drug Discov* 2018; 17: 395–412.